

REGIONAL CLIMATE MODEL SIMULATIONS OF PRESENT-DAY AND FUTURE CLIMATES OF SOUTHERN AFRICA

Hadley Centre technical note 39

D. A. HUDSON and R. G. JONES

13 August 2002



REGIONAL CLIMATE MODEL SIMULATIONS OF PRESENT-DAY AND FUTURE CLIMATES OF SOUTHERN AFRICA

D. A. HUDSON and R.G. JONES

Met Office, Hadley Centre for Climate Prediction and Research, London Road, Bracknell, RG12 2SY, U.K.

ABSTRACT

The Hadley Centre Regional Climate Model (RCM), HadRM3H, is run over southern Africa with the aim of examining climate change scenarios for the future. The model has a ~50 km resolution and is forced at its lateral boundaries by a high resolution (~150 km) atmosphere-only GCM, HadAM3H. The present-day simulation with the RCM (1961-1990) is evaluated, including an examination of the impact of enhanced resolution and an identification of biases in the RCM climate. The RCM is able to resolve features on finer scales than those resolved by the GCM, particularly those related to improved resolution of the topography, such as its influence on surface air temperature and large-scale precipitation. The regional model, unlike the GCM, is also able to resolve tropical cyclones, which affect eastern tropical regions of southern Africa in summer. The hydrological cycle is stronger in the RCM, with consequent increases in the intensity of rainfall, in the magnitude of the moisture fluxes and in soil moisture compared to the driving GCM. The largest errors in temperature and precipitation in the RCM (and GCM) control climate occur in summer. There are positive biases in precipitation, and negative biases in surface air temperature over much of southern Africa in this season. These errors are due to errors in both the internal model physics and the lateral boundary conditions inherited from the GCM. An additional RCM experiment, where the model is forced by reanalysis data (i.e. quasi-observed) aids in the identification of the sources of these errors. A 30-year (2071-2100) RCM climate change experiment (using the A2 emissions scenario) demonstrates a mean surface air temperature increase of 3.7°C in summer and 4.0°C in winter over southern Africa by the 2080s. The regional model predicts a drying over much of the western subtropical subcontinent in summer, associated with a decrease in both the number of rain-days and the intensity of rainfall. In contrast, equatorial regions tend to become wetter, due here to an increase in rainfall intensity rather than a change in the number of rain-days.

1. INTRODUCTION

Global Climate Models (GCMs) are the most appropriate tool for addressing future climate change. However, in order to formulate adaptation policies in response to climate change impacts, reliable climate change information is usually required at finer spatial scales than that of a typical GCM grid-cell (which is usually about 300 x 300 km). Thus, although GCMs provide adequate simulations of atmospheric general circulation at the continental scale, they do not capture the detail required for regional and national assessments. This is particularly true for heterogeneous regions, where sub-GCM grid-scale variations in topography, vegetation, soils and coastlines have a significant effect on the climate. In addition, at coarse grid resolutions extreme events such as cyclones or heavy rainfall are often not captured, or their intensity is unrealistically low. One solution is to use a Regional Climate Model (RCM), which will provide finer spatial and temporal detail than the GCM. Like a GCM, it is a comprehensive physical model representing the important components of the climate system. It has a higher resolution than a GCM and covers a limited area of the globe. The RCM is “nested” within a GCM. At its lateral boundaries the RCM is driven by winds, temperature and humidity variables output every 6 hours from the GCM. This is referred to as one-way nesting, since the RCM does not feed information back to the GCM.

In the time between the IPCC (Intergovernmental Panel on Climate Change) second (IPCC, 1996) and third (IPCC, 2001) assessment reports there has been a marked increase in the number of RCM simulations. However, there have been very few RCM studies done over southern Africa. To date, Sun *et al.* (1999a,b) used a 60 km resolution RCM (RegCM2 from NCAR, USA) to investigate rainfall over eastern Africa, and Joubert *et al.* (1999) examined the summer climate of southern Africa in a 125 km resolution RCM (DARLAM from CSIRO, Australia). Neither of these studies addressed future climate changes. Most regional modelling studies have tended to focus on areas of the Northern Hemisphere and Australia (for a list of references and details of RCM studies that have been performed, refer to Chapter 10 in IPCC, 2001). This is partly due to the computer-intensive nature of running regional climate models, such that most southern African research institutions do not have access to the necessary technology.

This report evaluates the RCM control simulation over southern Africa, drawing attention to errors in the simulation, as well as the effect of the increase in resolution compared to the driving GCM. The climate change scenarios produced by the RCM are then examined, with emphasis placed on changes in mean temperature and precipitation. Changes in extremes of climate are addressed in Hudson (2002).

2. EXPERIMENTAL DESIGN

The RCM (HadRM3H) is forced at its lateral boundaries by a high resolution GCM (150 km) called HadAM3H in so-called “time slice” experiments. HadAM3H is an atmosphere-only model which has been derived from the atmospheric component of HadCM3 (Gordon *et al.*, 2000; Pope *et al.*, 2000), the Hadley Centre’s state of the art coupled model which has a horizontal resolution of 3.75° latitude by 2.5° longitude. The idea is that a high resolution atmosphere-only GCM can be used to obtain an improved regional-level simulation over specific periods of interest identified from the coupled model integration. At this stage, it is computationally too expensive to run these high resolution GCMs themselves over century-long integrations. In the present experiments, two periods or time slices, namely 1961-90 and 2071-2100, have been selected from transient simulations (1860-2100) with HadCM3 (the HadCM3 simulations are described by Johns *et al.*, 2001). Observed time-dependent fields of SST and sea-ice (HadISST1 dataset, Rayner *et al.*, 2002) are used as lower boundary conditions in the control simulation with HadAM3H. In the climate change experiments, the HadCM3 SST anomaly is added to the observed data to use as the lower boundary forcing. Time-dependent greenhouse gas and aerosol concentrations are the same as in the corresponding HadCM3 time slice, and initial atmospheric and land surface conditions are interpolated from HadCM3. The development of HadAM3H is described by Jones *et al.* (1999) and Murphy *et al.* (2002). HadAM3H has been favoured over HadCM3 for driving the RCMs, since it has a higher resolution and exhibits an improved control climate, especially with respect to the positioning of the storm tracks of the Northern Hemisphere (Jones *et al.*, 1999, Murphy *et al.*, 2002). The representation of clouds and condensation, and the impact of land-surface physics on surface temperatures are also substantially improved (Jones *et al.*, 1999). HadAM3H has thus been used to drive the southern African RCM over the two time slice periods. An ensemble of three HadAM3H runs for the period 1961-1990, three simulations for the A2 future scenario (2071-2100) and one simulation for the B2 future scenario (2071-2100) have been run and assessed by Hudson and Jones (2002). One of the HadAM3H runs from the present-day period and one of the runs from the A2 scenario have been used to drive the southern African RCM.

3. MODEL DESCRIPTION

The southern African RCM (HadRM3H) has been configured for a domain extending from about 45°S to the equator and 5°E to 55°E. In the choice of an RCM domain, it is desirable to select a domain that is both large enough that the regional model can develop its own internal regional-scale

circulations, but not too large that the climate of the RCM deviates significantly from the GCM in the centre of the domain. Sensitivity simulations were performed in order to determine an appropriate domain size. Two “small” domains were tested, both extending from about 40°S to 12°S and 9°E to 43°E, but with one having a 0.44° resolution (~50 km) and the other a 0.22° resolution (~25 km), as well as a large domain (45°S to 0° and 5°E to 55°E) at 0.44° resolution. The test simulations highlighted a general insensitivity to domain size. As such, it was decided that a domain extending to the equator, would be scientifically interesting, as well as politically expedient, even though it is reasonably computationally expensive (in terms of computer time and data storage).

The horizontal resolution is 1.24° latitude × 1.88° longitude in the driving GCM (HadAM3H) and 0.44° × 0.44° in the RCM (HadRM3H). With a nominal resolution of 50 km versus 150 km, the RCM provides a more realistic representation of orographic features over southern Africa (Figure 1). The models employ spherical polar coordinates on a regular latitude-longitude grid, but in the RCM the pole is shifted to 67.5°S and 30°E in order to obtain quasi-uniform resolution over the area of interest. Both models have 19 layers in the vertical, which are based on a hybrid vertical coordinate (Simmons and Burridge, 1981). The timesteps are 15 minutes in the GCM and 5 minutes in the RCM. The GCM and RCM use the same grid scale dynamics and sub-grid scale physics, except for certain parameterisation constants which require different scaling in the RCM to account for the higher resolution (Jones *et al.*, 2001). A more complete description of HadRM3H is provided by Jones *et al.* (2001).

A one-way nesting procedure is used, with lateral boundary conditions for the RCM being specified by the GCM. The lateral boundary coupling occurs across a linearly-weighted 4-point buffer zone at each vertical level. The RCM is driven at its lateral boundaries by relaxing surface pressure (p^*), the horizontal wind components (u and v on the 19 model levels) and cloud-conserved temperature and moisture variables (θ and q_t on the 19 model levels) towards values interpolated in time from data saved every 6 hours from the GCM integration. Orographic heights in the RCM are equal to those in the GCM in the 4-point buffer zone, as well as the 4 rows/columns immediately within it (referred to as the 8-point buffer zone).

Various surface boundary forcing fields are required to drive the RCM. Prescribed observed SSTs are obtained by temporal interpolation from monthly mean fields of the Hadley Centre 1° × 1° resolution HadISST1 dataset (Rayner *et al.*, 2002). Lakes Tanganyika and Malawi are present in the RCM grid, but not in the GCM. No SST data were available for these lakes in the SST analyses, thus lake surface temperatures have been derived by interpolating values at the same latitudes from the surrounding oceans. The resulting values were compared with discontinuous observations of lake temperature for a few stations reported in the literature (Griffiths, 1972; Verburg *et al.*, 1998) and were deemed acceptable. Future SSTs are obtained by adding the HadCM3 SST anomaly to the observed data. The land-sea mask and surface topography are derived from the US Navy 10-minute resolution dataset, and spatially-varying vegetation and soil properties for the land surface scheme are prescribed from the 1° × 1° climatology of Wilson and Henderson-Sellers (1985). Initial conditions for the RCM (including atmospheric prognostic variables, soil and canopy moisture contents, deep soil temperatures and snow amount) are interpolated from the GCM timestep corresponding to the start date of the RCM simulation.

4. CONTROL CLIMATE SIMULATED BY THE RCM

4.1 COMPARISON OF RCM AND DRIVING MODEL CLIMATOLOGIES

In an RCM simulation it is desirable to firstly reproduce the mean circulation of the driving GCM, and secondly resolve features on finer scales than those accurately resolved by the GCM. This

section evaluates the control simulation of the RCM with respect to deviations from the simulated climate of the driving GCM, in essence highlighting the impact of an increase in resolution. The performance of the GCM is documented by Hudson and Jones (2002).

Table 1 summarises the 1.5m air temperature statistics over land points for the $0.5^\circ \times 0.5^\circ$ resolution CRU climatology (New *et al.*, 1999), the GCM and the RCM. For the analysis, the GCM and observed CRU data are interpolated to the RCM grid (which has the 8-point buffer zone removed), and only land points are used in the interpolation. It is important to note that the CRU data may suffer from errors in certain areas due to inadequate station coverage e.g. in Angola and the Democratic Republic of Congo (New *et al.*, 1999). Mean surface air temperatures over the land are slightly lower in the RCM compared to the GCM in all seasons (differences range from 0.18°C in summer to 0.93°C in winter). In summer (DJF) and autumn (MAM) this serves to slightly enhance the cold bias that was seen in the GCM, whereas in winter (JJA) and spring (SON) the warm bias is reduced (Table 1). The root-mean-square error results show that the largest errors (about 2°C) in both the RCM and GCM are found in summer. In all seasons the RCM has a higher spatial standard deviation in temperature than the GCM, related to increased fine-scale detail associated with the land surface and topography.

It is useful to be able to compare the RCM with the GCM and observations at scales resolved by the GCM, as well as evaluating the extra detail captured by the RCM at finer scales. To this end, the RCM and CRU data have been divided into large-scale and mesoscale components (this approach has been used by Jones *et al.*, 1995 and Noguier *et al.*, 1998). The large-scale component is obtained through aggregation of the data to the scale of the GCM, by averaging all land points lying within each GCM grid box, and the mesoscale component is obtained by calculating the difference between the large-scale component and the original data. Table 1 shows the spatial correlations between the various large-scale components, as well as the mesoscale components of the RCM and the CRU climatology. Both the RCM and GCM capture the basic large-scale temperature patterns in all seasons, with correlations not below 0.73. The large-scale patterns of the RCM and driving GCM are highly correlated (correlations do not fall below 0.94). This is what we would expect, especially since there is a high degree of compatibility between the models in terms of their physics and dynamics schemes. The RCM is able to capture the spatial patterns of the observed mesoscale signal (correlations do not fall below 0.8), and also reproduces the portion of this signal associated with orography, i.e. the negative correlation with orographic height (due to the decrease in atmospheric temperature with altitude). These impacts of improved resolution in the RCM can be clearly seen in the temperature difference field between the RCM and GCM in, for example, summer (Figure 2). The differences largely mirror differences in the topography and coastal resolution (Figures 1 and 2). Improved definition of the major river valleys can be seen as warmer areas in the RCM compared to the GCM, particularly for the Zambezi river valley. More pronounced though, are the effects of the improved resolution of the narrow coastal plain and steeply rising escarpment over the east coast of South Africa, portions of the west coast of southern Africa, and the east coast of Madagascar. This results in warmer coastal regions and cooler mountainous areas in the RCM compared to the GCM. All the mountainous areas are mirrored in the difference fields as showing cooler temperatures in the RCM. In many of these areas the difference in model topography between the GCM and the RCM exceeds 300 m.

Statistics for precipitation have been calculated in the same way as for temperature and are presented in Table 2. Precipitation is greater in the RCM over the land in all seasons compared to the GCM, with largest absolute differences in summer and autumn (both exhibit 0.8 mm/day more rain in the RCM). The root-mean-square error results show that the largest errors in precipitation are in summer for both the GCM and RCM (3 mm/day for the RCM and 1.9 mm/day for the GCM). The GCM and RCM capture the large-scale patterns of the CRU climatology relatively well (the lowest correlation is 0.63), but the RCM shows little skill in reproducing the mesoscale component

(correlations range from 0.15 to 0.26). The correlations of the observed mesoscale component of precipitation with orography are small, as are the corresponding correlations between the RCM and orography. In both the model and observed, these correlations are larger in summer compared to winter. In summer, mountainous terrain may provide an elevated heat source and increase the potential for localised convection (coupled with day-time anabatic flow and up-slope convergence). In winter, most of southern Africa is very dry and with such small rainfall totals it is difficult to achieve meaningful correlations. If, however, just the subtropical western section of southern Africa is considered (extending to 15°S and 24°E), which receives rainfall in winter, then the correlation between the mesoscale components of the model and CRU climatology increases to 0.66 and the correlations with mesoscale orography are 0.45 and 0.33 for the model and CRU climatology respectively, as opposed to virtually no correlation when the whole of southern Africa is considered (Table 2). The generally weak correlations between the model and observed mesoscale fields may be largely due to too much noise at the grid-scale level of the RCM, as is suggested in Figure 3. This may indicate that the RCM is too sensitive to the mesoscale variations in orography and could perhaps be improved by running the RCM using smoothed orography.

In the RCM there is more convective and large-scale precipitation over land and sea points throughout the seasonal cycle compared to the GCM, particularly in the summer months (Figure 4). The enhancement of precipitation in summer in the RCM occurs over large areas of the subcontinent (Figure 5). The difference over land areas is equivalent to a 20% increase in precipitation. The results suggest that the hydrological cycle is more active in the RCM compared to the driving GCM. Moisture fluxes from the surface into the atmospheric boundary layer are higher over both land and sea in the RCM (Figure 6), there is more precipitation (Figure 5), and the root-zone soil moisture content is larger (Figure 7). There is also a larger sensible heat flux from the surface into the atmospheric boundary layer (probably due to higher boundary layer wind speeds and more incident surface shortwave radiation in the RCM) over large regions of the land (not shown), which causes a positive feedback on precipitation, since there is greater heating and moistening of the boundary layer and thus potentially more instability in the RCM. In general, the intensity of precipitation in summer is higher in the RCM compared to the GCM (Figure 8). Over coastal and eastern regions there are more rain-days in the RCM, but over central western regions there are fewer (Figure 8). The implications are that in the RCM the transfers of moisture stores are happening faster than in the GCM. Precipitation increases in the RCM are also associated with more resolved ascent (discussed in the following paragraph). In addition, deviations in the circulation of the RCM from the driving GCM contribute to the land precipitation. For example in summer the 850 hPa wind anomalies show stronger low level easterly winds off the south-west Indian Ocean (south of Madagascar) in the RCM, which would advect more moisture over the land (not shown).

Increases in large-scale rainfall can be seen primarily over the mountains of Madagascar and the South African escarpment (Figure 5). These increases over the mountains are largely due to the finer resolution causing enhanced topographical forcing and dynamical uplift. As expected during the summer season, most of the increases in rainfall over the interior of southern Africa are convective in origin (Figure 5). Over north eastern regions of the subcontinent there is a mixture of positive and negative convective rainfall anomalies in the difference field. This may be due to the influence of the increased resolution of the complex topography in that area, and the impact that that may have on local-scale diurnal heating and the convergence/divergence of airstreams. Rainfall over eastern Africa is known to exhibit complicated spatial patterns. There is a notable increase in convective rainfall in the Mozambique channel in the RCM (Figure 5), and a corresponding decrease in sea level pressure (~1.5 hPa, not shown). In summer this area is affected by tropical cyclones, with between six and twelve storms per year occurring over the SW Indian Ocean, and about one to five passing south between Madagascar and Africa (Tyson and Preston-Whyte, 2000). It is possible that in the RCM there is improved resolution of these storms, causing

them to be more intense and persistent. An examination of daily sea level pressure fields in the RCM and GCM suggest that this is the case (for example, Figure 9). Clearly, the ability of the model to simulate these cyclones is very important to climate impacts of countries such as Mozambique and Madagascar. Hudson (2002) found that the RCM does relatively well in capturing the structure of tropical cyclones, but initial indications suggest that it may be simulating 3-4 times too many cyclones in the Mozambique Channel compared to observed.

The RCM is also characterised by stronger vertical velocities than the driving GCM (Figure 10), mainly due to improved resolution of smaller scale features of the dynamics (e.g. storms) and also its interaction with topography. This is alluded to in winter (JJA), where there is an increase in large-scale precipitation over Cape Town and the east coast of South Africa in the vicinity of the Drakensberg escarpment (Figure 11). The south western region of South Africa receives its rainfall during winter due to the passage of cold fronts. Figure 12 shows that the RCM does better than the GCM in capturing the observed distribution of daily rainfall. This is probably due to improved resolution of the complex topography and coastline of the South Western Cape in the RCM compared to the GCM, since the interaction between atmospheric circulation and topography has an important influence on rainfall in the region. The increase in large-scale rainfall south-east of South Africa over the Indian Ocean (Figure 11) is also probably due to improved resolution of the smaller-scale features of midlatitude depressions and their associated cold fronts that pass over the region in winter.

It was shown in the previous report that the GCM overestimates cloud cover over much of southern Africa during summer and winter (Hudson and Jones, 2002). The RCM tends to reduce this positive anomaly, by generally simulating less total cloud cover, especially over the western and southern subcontinent (Figure 13). Cloud cover is, however, larger in the RCM than the GCM over certain coastal and high relief areas, for example parts of north eastern southern Africa and Madagascar. It is also higher over large areas of the Indian Ocean in summer, probably related to improved resolution of tropical cyclones. The reductions in cloud cover over large areas where there are increases in precipitation in the RCM may be related to a reduction in the lifetime of the cloud with the more rapid cycling of water in the RCM compared to the GCM.

This section has focused on how the RCM modifies the simulated climate of southern Africa compared to the driving GCM by virtue of its higher resolution. Although many of the changes that the RCM produces are more realistic and justified, often the bias with respect to observed is increased e.g. with summer precipitation. We need to look a bit more closely at the origin of such errors in the RCM.

4.2 ASSESSMENT OF THE RCM ERRORS

Errors in the RCM simulation are due to errors both in the lateral boundary conditions and the model physics. In order to analyse these errors an additional 15-year RCM simulation has been performed where the RCM is forced by ERA reanalysis data i.e. representing quasi-observed boundary conditions, using the method described by Taylor *et al.* (2001). The RCM simulation described in the previous section of the report, i.e. the RCM driven by GCM lateral boundary data, hereafter referred to as RCM CON, is compared to the RCM forced by ERA reanalysis data, hereafter referred to as RCM ERA. The two RCMs are thus identical apart from their driving data. The intention is to be able to partition the RCM errors; those biases that appear in both RCM CON and RCM ERA are ascribed to internal model errors, whereas those that appear only in RCM CON are ascribed to errors inherited from the forcing GCM through the lateral boundaries. However, it is not as simple as this in reality, since feedbacks occur that may act to exacerbate or diminish the initial model response.

This section will focus on summer, since this is the season when errors in temperature and precipitation tend to be largest, and it is when most of the subcontinent receives its rainfall. Temperature in the models is compared to the CRU climatology (New *et al.*, 1999), and precipitation to the CMAP precipitation analysis (Xie and Arkin, 1997). There are similar patterns of surface air temperature error in both RCM experiments, namely a cold bias over much of the subcontinent (Figure 14). However, the bias is accentuated in RCM CON, especially in the subtropics. There is also a relative warm bias in RCM CON over north-eastern southern Africa compared to RCM ERA (Figure 14). In both RCM experiments there is a wet bias over most of southern Africa (Figure 15), but there are a number of differences in the biases from the two experiments. The primary differences are that in RCM CON it is relatively:

- wetter over the Mozambique Channel and parts of north-eastern southern Africa
- wetter over subtropical southern Africa (notably in a NW-SE axis over South Africa, Namibia and Botswana)
- dryer over north-western equatorial/tropical Africa, such that in many cases there is a dry bias in RCM CON where there is a wet bias in RCM ERA.

Area-averaged precipitation over land areas is 52% higher than observed (CMAP data) in RCM ERA, 60% higher in RCM CON and 39% higher than observed in the driving GCM over the southern African domain in summer.

The following discussion of the RCM errors has been split into two sections; errors due to internal model physics, and those due to lateral boundary forcing, although in reality, as mentioned above, partitioning due to these sources is more blurred.

4.2.1 Internal model errors

In both RCMs there is a general cold bias over most of southern Africa (Figure 14). The common overlap of these errors in both experiments suggests that they are due to errors in the internal model physics. In the GCM, the error was partly ascribed to a positive bias in optically thick cloud, resulting in a reduction in the shortwave radiation reaching the earth's surface (Hudson and Jones, 2002). In the RCMs there is also an excess of thick cloud (optical thickness > 25 ; as defined in the ISCCP data (Rossow and Shiffer, 1991)) over most of the land (Figure 16), but the effect on the shortwave cloud forcing south of about 15°S (Figure 17) and incident solar radiation (Figure 18) is not as strong as in the GCM, and there are actually areas in both RCMs, especially RCM ERA, experiencing positive biases in incident surface shortwave radiation (Figure 18). Over south-western regions (south of $\sim 15^{\circ}\text{S}$ and west of $\sim 25^{\circ}\text{S}$) the cold bias may be related to the positive precipitation bias (Figure 15), which could cause an increase in evaporative cooling compared to observed. In this region the model soil moisture content at the beginning of summer is low (in winter the soils dry out such that soil moisture is generally less than 40 cm, but with extensive areas less than 10 cm), thus most of the soil moisture and evaporation that occurs during summer comes from the rainfall that falls in summer (model P-E values are generally less than ± 1 mm/day). A comparison of the model-derived evaporation with observed summer precipitation shows that evaporation from the model exceeds observed precipitation south of $\sim 15^{\circ}\text{S}$ (by up to 4 mm/day). This suggests that the model evaporation is greater than observed evaporation over these moisture limited regions, leading to greater evaporative cooling.

There is a general wet bias over southern Africa in both RCMs in summer (Figure 15). This bias may be partially related to errors in the equatorial/tropical region ($5\text{--}15^{\circ}\text{S}$). In this region, total cloud cover is greater than observed, but medium thickness clouds (optical thickness 3 – 25; as defined in the ISCCP data (Rossow and Shiffer, 1991)) (especially those with middle to high-level cloud tops, i.e. anvil cirrus) are under-represented (Figure 19). Although there is more optically thick cloud than observed in this region (Figure 16), this does not compensate for the underestimate of medium thickness clouds, since shortwave cloud forcing is less than observed in

equatorial/tropical land regions (positive values in Figure 17) and more insolation reaches the earth's surface (Figure 18). This process could increase the heat low influence, deepen the trough and result in the stronger recurved westerlies off the Atlantic Ocean (Figure 20). This would contribute to increased moisture convergence into the Intertropical Convergence Zone (ITCZ) and the positive rainfall bias over the land. This hypothesis is currently being tested in a series of sensitivity experiments with the RCM which alter parameterisations in the convective cloud scheme in order to increase cloud optical thickness in the ITCZ. Initial results indicate that this change does indeed reduce the precipitation bias over southern Africa.

It is also possible that some of the RCM errors may be related to an inadequate representation of the land surface. The model currently uses spatially-varying vegetation and soil properties from the $1^\circ \times 1^\circ$ climatology of Wilson and Henderson-Sellers (1985). However, this dataset does not vary temporally, and seasonal variations in surface albedo, roughness and leaf area index could have a significant affect on the climate.

4.2.2 Errors introduced through the lateral boundaries

The primary difference in the errors of the two RCM experiments appears in the wind and pressure fields. RCM CON displays consistently larger wind and pressure deviations from observed, with the three primary moisture feeds for the subcontinent all being enhanced (as was seen in the GCM) (Figure 20). Of particular note is the strong anticyclonic anomaly over the Indian Ocean south of Madagascar at the 300 hPa level in RCM CON. This results in stronger divergence ahead of the trough axis of the upper level wave, as can be seen in the 200 hPa divergence anomaly field (Figure 21). This situation, coupled with the convergence anomaly at the 700 hPa level (not shown, but stronger than that of RCM ERA), promotes deep uplift and favours anomalous rainfall in a NW-SE orientation across Namibia, Botswana and South Africa (Figure 15). These anomalies would account for the larger precipitation anomalies seen in RCM CON compared to RCM ERA over subtropical southern Africa (Figure 15). There is also a pronounced low-level cyclonic anomaly in the Mozambique Channel in RCM CON, as well as enhanced divergence at the 200 hPa level, with a resulting excess of precipitation (Figures 15, 20 and 21).

In RCM CON there is a drying over north-western southern Africa (Figure 15). This error is visible in RCM ERA, but is much more restricted in areal extent. Amplification of the error in RCM CON is possibly due to the enhanced low-level westerlies off the Atlantic (Figure 20) causing a divergence anomaly over the region (not shown).

Enhancement of the cold bias over South Africa, Botswana and Namibia in RCM CON (Figure 14) is probably due to cloud differences, such that there are more extensive negative anomalies of incident surface shortwave radiation in RCM CON compared to RCM ERA (Figure 18).

In general, the circulation biases that are inherited from the GCM via the lateral boundaries of the RCM's domain serve to transport more moisture over southern Africa, thus contributing to the positive rainfall bias that is evident in RCM CON over much of the sub-continent in summer. The key to reducing most circulation errors lies in improving the driving GCM.

Although there are important systematic errors in certain variables in the RCM, most of the spatial features of the seasonal circulation over southern Africa are reasonably represented by the model. The preceding evaluation of the performance of the control simulation is essential before the model can be used in climate change experiments. Errors in the present-day simulation may affect the model response to various forcings, and need to be considered when analysing the climate change signal and applying the results to impacts assessments.

5. CLIMATE CHANGE

A single 30-year climate change simulation, using the A2 SRES emission scenario, has been performed with the RCM. In contrast, a three member ensemble is available for the A2 scenario from the GCM (HadAM3H), as well as a single simulation for the less severe B2 scenario. The results of these simulations are documented in Hudson and Jones (2002). In this section, temperature and precipitation results are shown for the driving GCM as well as the RCM since their climate change response may differ and it is important that this is assessed. Unless otherwise mentioned, the GCM A2 scenario results presented are for the single realisation that forces the RCM, and not the ensemble mean. Other GCM scenario simulations (e.g. the B2 simulation) are also shown in order to place the results obtained from the RCM in perspective. Figure 22 shows the change in surface air temperature over land points in the southern African domain as simulated by the Hadley Centre's fully coupled ocean-atmosphere GCM (HadCM3) (Johns *et al.*, 2001) for four of the SRES emissions scenarios developed in the IPCC Special Report on Emission Scenarios (IPCC, 2000). The figure places the B2 and A2 scenarios in context, showing resulting temperature increases over southern Africa ranging between about 2° and 6.5°C by 2100, associated with the less and more extreme B1 and A1FI scenarios respectively. The discussion below focuses on the mean surface air temperature and precipitation response to climate change. Changes in extremes are considered in Hudson (2002).

5.1. Surface Air Temperature

The seasonal cycle of surface air temperature is shown in Figure 23 for the RCM and GCM (all ensemble members shown) control and A2 simulations, as well as the B2 simulation from the GCM. The data are represented as spatial averages over the 6 land regions shown in the figure. The GCM results (solid lines) show that as one might expect the temperature increase relative to the controls is smaller in the B2 simulation compared to the A2 simulations, due to the weaker emission forcing in the B2 scenario. In all regions the results suggest a linear response to the emission forcing. The GCM control and A2 simulations show that there is a large degree of coherence between the members of the ensemble (sometimes they are indistinguishable), implying a high signal-to-noise ratio in the temperature response. The RCM (dashed lines) simulates a similar magnitude of temperature change in response to the A2 scenario forcing as the GCM, but the temperature in the RCM is slightly lower than the GCM for both the control and future simulations. In general, the largest discrepancies between the global and regional models is found in the summer half of the year and north of 25°S. Neither the RCM or GCM suggest any shifts in the seasonal cycle in response to climate change.

As has been found in other models (IPCC, 2001), the surface air temperature response over the southern African domain is larger over the land than the adjacent oceans in both the RCM and GCM, and is probably the result of less evaporative heat loss over the land, as well as the greater thermal inertia of the oceans. A comparison of the GCM mean temperature change over land with the global mean change obtained from the GCM (Table 3), shows that in general southern African land areas warm slightly more than the global mean, particularly in autumn and winter. These results can be compared with those of Giorgi *et al.* (2001), who analysed the consistency of nine different ocean-atmosphere GCMs in terms of regional warming for different areas of the globe relative to each model's global warming under the A2 and B2 scenarios. For the nine models assessed, the global annual average warming ranged from 0.9° to 3.4°C for the B2 scenario and 1.2° to 4.5°C for the A2 scenario (Giorgi *et al.*, 2001). The values obtained from HadAM3H fall within the upper half of each of these ranges (2.30°C for the B2 scenario and 3.14°C for the A2 scenario). Over southern Africa they found agreement (at least 7 out of the 9 models) on warming greater than the global average (but not in excess of 40% of the global warming) for the A2 and B2 scenarios in

winter (JJA), as found in the present study (Table 3, but not shown for B2), but inconsistent magnitudes of warming were obtained for summer (Giorgi *et al.*, 2001).

Figure 24 shows the pattern and magnitude of temperature increase for each season for the GCM B2 and A2 scenario results and the RCM A2 scenario results. As shown previously, the temperature increase predicted for the A2 scenario is larger than the B2, but there is a very similar pattern of change for both scenarios (pattern correlations between the GCM B2 and A2 scenarios are 0.97 for DJF and MAM, and 0.98 for JJA and SON). The pattern of temperature change can be explained by various feedbacks. For example, in summer the surface temperature increase over the land is largest over the western half of the subcontinent, and smallest in the vicinity of Kenya and Tanzania. Over Kenya and Tanzania the smaller temperature increase appears to be the result of a negative feedback induced by increased cloudiness (of thick cloud especially), causing an increase in shortwave cloud forcing, and a reduction in insolation reaching the earth's surface. In addition, there is an increase in the surface moisture flux in this region, which would result in greater evaporative cooling. In contrast, over the western half of the subcontinent the temperature increase is enhanced by a positive feedback resulting from a reduction in thick cloud cover and shortwave cloud forcing, causing an increase in shortwave radiation reaching the earth's surface. The temperature increase is also enhanced by the reduced surface moisture flux in this region resulting in less evaporative cooling. These changes are discussed in more detail by Hudson and Jones (2002).

The third column of Figure 24 shows the RCM prediction for the A2 scenario. The RCM produces similar changes in terms of magnitude and pattern to the GCM simulation. Table 3 shows that the GCM and RCM response patterns are highly correlated in each season (correlations do not fall below 0.88), and that the correlation of the large-scale component (calculated as in section 4) of the RCM with the GCM is even slightly higher (correlations do not fall below 0.90). The mesoscale component of the response, apparent in Figure 24, is relatively small, only accounting for about 7% of the spatial variance of the RCM mean response (Table 3). A similar result was found using a previous version of the RCM over Europe, where the mesoscale component contributed around 10% of the spatial variance of the mean response (Jones *et al.*, 1997). There are, however, a number of differences in the GCM and RCM response. For example, in summer the RCM generally produces a smaller temperature increase over southern land areas (predominantly south of about 20°S), but an enhanced warming over western tropical and equatorial regions (Figure 25). This may be partly related to the stronger hydrological cycle in the RCM. An examination of the surface moisture flux anomalies (Figure 25) shows that the RCM has generally larger anomalies than the GCM. The greater reduction in the moisture flux over western tropical and equatorial regions will enhance the warming relative to the GCM, whereas the larger flux increase, and thus more evaporation over southern portions of the subcontinent, will reduce the warming compared to the GCM.

Finally, in order to place the RCM results in context, Figures 26 and 27 show the summer and winter temperature change over southern Africa under the A2 emissions scenario as simulated by coupled ocean-atmosphere GCMs from other institutions, as well as two Hadley Centre models: HadCM3, the coupled ocean-atmosphere GCM; and HadAM3H, the high resolution atmosphere-only GCM used to drive the RCM. Unfortunately there are no other RCM studies over southern Africa with which to compare the results. There is a large spread in the various model results, in terms of both pattern and magnitude, thus emphasising the uncertainty in the regional response. This illustrates the potential danger in relying on the results from a single model. It is interesting to note that there are even differences in the response between the two Hadley Centre GCMs, particularly in winter. HadAM3H was derived from the atmospheric component of HadCM3, but there are a number of differences between them. These include a doubling in horizontal resolution, changes in cloud and condensation parameterisation and changes to the coupling between the soil

and land surface (Jones *et al.*, 1999). The differences between the climate change signal in the two GCMs are likely to be largely due to differences in cloud distributions and feedbacks.

5.2. Precipitation

The seasonal cycle of precipitation for the RCM and GCM control and future simulations is shown in Figure 28. It is evident that there is a larger degree of variability between simulations within an ensemble (i.e. for the GCM control and A2 scenario) compared to temperature (Figure 23). Summer rainfall decreases over western equatorial and tropical regions as the scenario forcing increases (i.e. B2 to A2) and the results suggest a linear response, but this is not as clear for the other regions. The RCM (dashed lines) generally produces more rainfall than the GCM for both the control and A2 scenario. As for temperature, there do not appear to be any major shifts in the seasonal cycle under climate change.

The area-averaged precipitation change over land in summer is small; GCM changes range from a 3% decrease under the B2 scenario (not shown) to a 5% decrease under the A2 scenario (the RCM produces a 1% decrease under the A2 scenario) (Table 4). In winter the changes are larger, ranging from a 16% decrease under the B2 scenario (not shown) to a 24% decrease under the A2 scenario (the RCM produces a 30% decrease under the A2 scenario) (Table 4). In a comparison of nine ocean-atmosphere GCMs, Giorgi *et al.* (2001) found that there was disagreement between the models as to the summer precipitation change over southern Africa for both the A2 and B2 scenarios (i.e. an inconsistent direction of change, outside the -5 to 5% “no change” category), whereas for winter there was agreement on a small decrease (-5 to -20%) under both scenarios. It is important to remember that reporting percentage changes in winter for southern Africa can be misleading because there is very little rainfall in this season (the GCM control mean for winter is 0.44 mm/day, compared to summer where the mean is 5.42 mm/day), therefore although absolute changes may be small, the percentage changes are large.

The area-averaged response, however, masks the contrasting increases and decreases of rainfall that are found over different regions of the domain. Figure 29 displays the pattern and magnitude of precipitation change for each season for the GCM B2 and A2 scenarios and the RCM A2 scenario (changes significant at the 5% level are displayed). The GCM results show that the scaling of precipitation with the increasing emissions is not as clear as it was for temperature. For example, over the Indian Ocean north of Madagascar in autumn (MAM) there is a larger increase in rainfall in B2 scenario compared to the A2 scenario. One of the problems is the high variability of precipitation (as indicated in Figure 28), such that it is difficult to separate the signal from the noise. One way this can be overcome is by increasing the number of simulations (different initial conditions but using the same forcing scenario) and producing an ensemble mean response. The natural variability (“noise”) is reduced by averaging over the members in the ensemble, and a clearer climate change signal emerges. An ensemble of three simulations has been performed for the GCM A2 simulation, but there is only one simulation for the B2 scenario and the RCM A2 scenario. Nevertheless, there are clear patterns that emerge from the GCM (A2 and B2 scenarios) and RCM in response to the scenario forcing. In all seasons there is a tendency for an increase in rainfall over equatorial latitudes (especially over the eastern half of the domain), and a decrease in rainfall over the tropics and subtropics, particularly over western regions of the subcontinent.

Focussing on summer, the primary rainfall season, it is clear that for both the GCM and RCM there is a statistically significant increase in rainfall north of 10°S and east of 20°E under the A2 scenario (Figure 29). There appears to be enhanced convection under future conditions in this region. The warming of the atmosphere leads to an increase in specific humidity through an increase in evaporation, especially over equatorial regions, and this in turn contributes to enhanced low level

moisture convergence in this region (Hudson and Jones, 2002). These increases in precipitation are also generally associated with increases in the root-zone soil moisture content (not shown).

In contrast, there is a tendency for a decrease in rainfall south of about 10°S, but with statistically significant decreases over western and central land areas and largest absolute changes being between 10°S and 20°S in the vicinity of eastern Angola (the ~2 mm/day reduction translates to about a 20% reduction in rainfall) (Figure 29). The RCM shows smaller regions exhibiting a statistically significant decrease compared to the GCM. The general reduction in rainfall over the land south of about 10°S in summer, and particularly over western regions, is associated with a reduction in the root-zone soil moisture content, a reduction in cloud cover and a general reduction in evaporation (although there are regions of precipitation decrease where the moisture flux increases) (Hudson and Jones, 2002). The GCM results demonstrated that circulation changes may be contributing to this reduction in rainfall over southern Africa (Hudson and Jones, 2002). There is increased subsidence in the troposphere between about 10°S and 25°S, especially at mid-tropospheric levels, and there is an anticyclonic anomaly at the 500 hPa level in the circulation field, centred over western regions of southern Africa south of about 10°S (Hudson and Jones, 2002). At the 850 hPa level, geopotential height changes indicate a strengthening of the South Atlantic and South Indian High Pressures, and a reduction in strength of the tropical low (centred over southern Angola and northern Namibia) and easterly wave (Hudson and Jones, 2002). Whetton *et al.* (2001) also report a reduction in rainfall in the subtropics over Australia, and suggest that it may be a consequence of a stronger hydrological cycle under climate change, which results in enhanced rainfall and ascent in the ITCZ (rising limb of the Hadley circulation) and increased descent and reduced rainfall in the subtropics (descending limb of the Hadley circulation).

The pattern of rainfall change in the RCM and GCM in summer (Figure 29) is very similar to the present-day precipitation response to El Niño events i.e. dryer than normal conditions over much of southern Africa, especially western regions, and above-normal rainfall over equatorial east Africa. The 30-year mean sea-surface temperature change in response to climate change, obtained from the Hadley Centre's coupled ocean-atmosphere GCM (HadCM3), exhibits an El Niño-like pattern of change in the Pacific, with greater warming in the eastern tropical Pacific (not shown). These are the SST anomalies that are used in the RCM and its driving GCM. The precipitation response over southern Africa may thus be linked to a shift towards an El Niño-like regime under the future climate change scenario. The El Niño-like change in Pacific SSTs has been found in other ocean-atmosphere GCMs, but the cause of the change remains uncertain (IPCC, 2001).

Table 4 shows that there are strong spatial correlations between the GCM and RCM response patterns for the A2 scenario (correlations do not fall below 0.75) and, as found for temperature, the correlation of the large-scale component of the RCM with the GCM is slightly higher (correlations do not fall below 0.83). There are, however, a number of differences between the A2 scenario response from the RCM and the GCM (Figure 29). Firstly, the increased level of detail is clear in the RCM results. The mesoscale component of the response accounts for about 20% of the spatial variance of the RCM mean response (Table 4), higher than that found for temperature. Secondly, for those regions where precipitation increases in the GCM, the RCM tends to simulate larger and more widespread increases in precipitation in each season compared to the GCM (Figure 29). This could be attributed to the stronger hydrological cycle in the RCM. It is apparent that although the large-scale general changes in precipitation are similar, if the results from the two models were used in an impacts assessment, e.g. investigating changes to water resources, then on a local to regional basis there may be large differences in the resulting impact.

As mentioned previously, it is important to remember that biases in the model control climate (RCM or GCM) may distort the climate change signal. For example, the reduction in rainfall over the south-west of the sub-continent is associated with a reduction in evaporation, and thus an enhanced

warming over the region. Western areas of South Africa, Namibia and southern Angola receive less than 2 mm/day under present-day conditions in summer. However, the model (GCM and RCM) simulates too much rainfall over this region (sometimes exhibiting a positive bias of more than 2 mm/day), and the rainfall reductions that are predicted under climate change are up to about 1.5 mm/day. Thus, the warming that is simulated under climate change conditions may be exaggerated in certain of these areas, due to the excessive latent heat fluxes that exist in the model. In other words, in the model there is more rainfall over this region in the control and possibly more evaporation compared to observed, therefore under the modelled climate change situation there is a reduction in rainfall and the evaporation of moisture that might not actually be available in reality.

Changes in the variability of rainfall may have a more significant impact on society than changes in the mean. Much of southern Africa experiences a high degree of intra- and interannual rainfall variability, and the region is particularly vulnerable to floods and droughts. In summer in response to the A2 scenario forcing, there is a decrease in the interannual variability of seasonal mean precipitation over western tropical and subtropical land areas, but an increase in variability west of Lake Tanganyika in the Democratic Republic of Congo in both the RCM and the GCM (Figure 30). The changes in variability tend to be more marked in the RCM. In winter, over most of Africa south of the equator there is a reduction in the interannual variability of seasonal mean precipitation. The RCM predicts a stronger reduction in variability than the GCM over the eastern half of South Africa (Figure 30). As has been found in other models (IPCC, 2001), there is a tendency for increases (decreases) in interannual variability in those regions where mean precipitation increases (decreases).

Analysis of daily precipitation in the RCM and GCM shows that in summer there is a general reduction in the number of rain-days over southern Africa (Figure 31), although there are key regions where the average intensity of rainfall increases (Figure 32). In fact, the increase in mean rainfall over equatorial latitudes is related to more to an increase in the intensity of rainfall rather than a change in the number of rain-days. In contrast, the decrease in mean summer rainfall over western and central land areas south of about 10°S, is related to a decrease in the number of rain-days, as well as a decrease in the average intensity of rainfall. Over the east coast of southern Africa, in the vicinity of southern Mozambique, the small changes in mean precipitation are masking the increases in average rainfall intensity combined with decreases in rain-day frequency. This may be important for impacts assessments and highlights the importance of examining daily rainfall variability and not only mean changes. For winter, the small reduction in mean rainfall over large regions of southern Africa is generally associated with reductions in both the number of rain-days and the rainfall intensity.

There is still considerable uncertainty in the regional response of precipitation to global climate change (IPCC, 2001). This is highlighted in Figure 33 and 34 which show the percentage change in precipitation under the A2 scenario from a selection of GCMs. There is a wide range of patterns and magnitudes of change, and it is difficult to detect a cohesive response (Figures 33 and 34). In an analysis of fully coupled ocean-atmosphere GCMs, Giorgi and Francisco (2000a,b) found that the largest source of uncertainty in regional changes was inter-model differences, although Hulme *et al.* (1999) note that high natural variability at sub-regional scales can obscure the climate change signal.

6. CAVEATS AND CONCLUSIONS

The RCM resolves features on finer scales than those resolved by the GCM. This is particularly clear for surface air temperature, where differences between the GCM and RCM largely mirror improvements in the resolution of the topography and coastline. In addition, there is more resolved ascent associated with large-scale precipitation and enhanced topographical forcing in the RCM.

The hydrological cycle is more active in the RCM, with moisture fluxes, the intensity of precipitation and the soil moisture content all being higher than in the GCM. The transfers of moisture stores appear to occur faster than in the driving GCM. An important advantage of the RCM over the GCM is its' ability to resolve tropical cyclones.

The regional model captures the primary features of observed circulation and pattern of seasonal change over southern Africa, but there are significant biases. Most noteworthy are positive biases in precipitation, and a negative bias in surface air temperature in summer over much of the subcontinent. These errors are also present in an RCM experiment which is forced by reanalysis ("quasi-observed") data, suggesting that they are due to errors in the internal model physics. The positive precipitation bias in the RCM may be related to an underestimate of cloud optical thickness in the ITCZ, resulting in a positive bias in incident surface shortwave radiation. This appears to enhance the heat low effect and increase the strength of the low-level recurved westerlies that enter southern Africa from the tropical Atlantic Ocean, thus bringing more moisture over the subcontinent than observed. The RCM is also influenced by errors in the large scale circulation of the driving GCM. The primary effect of these lateral boundary errors is to transport more moisture over southern Africa, and through circulation anomalies, to increase rainfall in a NW-SE orientation across Namibia, Botswana and South Africa. This increase in rainfall also exacerbates the cold bias through an increase in evaporative cooling in those regions that are moisture limited. The Hadley Centre's RCM has been extensively used and evaluated over the European domain, but this study highlights the importance of evaluating it over other regions where different processes may be more or less significant, for example convection is relatively more important over the southern African domain. This helps in the identification of model errors and leads to model improvement.

The RCM climate change results for the 2080s relative to the present-day under the A2 SRES emissions scenario indicate a mean annual increase of 3.88°C in surface air temperature over land points in the southern African domain. In summer over equatorial land regions there is a general increase in average rainfall and the intensity of rainfall (rather than the number of rain-days). Over western and central tropical and subtropical land areas, there is a reduction in average rainfall, in the number of rain-days and in the average intensity of rainfall. There are regions of eastern subtropical southern Africa where the mean summer rainfall decreases, but the intensity of rainfall on any given rain-day increases. In winter there is a general reduction in rainfall over the land, except for central equatorial longitudes.

There are a number of uncertainties and caveats associated with the RCM's predictions of climate change over southern Africa. Firstly, the climate change signal produced by the RCM is dependant on the large-scale circulation from the driving GCM. Any errors in the GCM response to the emission forcing will be transferred to the RCM. Secondly, this study relies on a single RCM simulation for the present-day and future period respectively. This means that natural variability may be obscuring the climate change signal, especially for precipitation where the changes are relatively small and the natural variability is large. Producing an ensemble of simulations for each period, and averaging the results over the ensemble, may increase the signal-to-noise ratio. Thirdly, there are differences in the regional response to climate change from different GCMs (and different results may be obtained from the present study if a different RCM were used). This uncertainty, due largely to differences in model physics, highlights the importance of assessing results from a variety of models for the production of impacts assessments, rather than relying on a single model. Lastly, the present study assesses regional changes from a single SRES emissions scenario. Ideally the study should be repeated using different emission scenarios. Alternatively, a method could be developed to scale the regional response from the A2 emissions scenario to the other emission scenarios.

Perhaps one of the most pertinent questions is whether or not the RCM climate change results should be used for impacts assessments in light of the systematic errors that are present in the control climate. This is a difficult problem to address, since it is not easy to quantify the extent to which biases in the control climate affect the climate change signal. It is probably not advisable to use the raw RCM output in impacts studies, particularly for variables such as precipitation which exhibit a fairly large bias. Instead, scenarios can be constructed by adjusting an observed baseline climate by the change between the control and future simulations. This is a commonly used approach in impacts studies. There is also the problem that the RCM sometimes produces different magnitudes and patterns of change in response to the emissions forcing compared to the driving GCM. Which model results should be used? The answer to this question is dependant on the type of impacts study being conducted, the region that is being considered and the variable(s) being used. For example, in a study of the impact of climate change on water resources in the winter rainfall region of the South Western Cape of South Africa, I would use the RCM data, since the regional model does considerably better than the global model in capturing the observed distribution of present-day rainfall and I would thus have more confidence in its' climate change predictions for the region. Similarly, if I were examining changes in extreme rainfall or storm surges over the east coast of southern Africa, I would probably use the RCM data, since unlike the GCM, the model is able to resolve the tropical cyclones which affect this region. In contrast, I would be cautious in using summer precipitation from the RCM for much of western southern Africa, since although the GCM also has positive biases in its' control rainfall, the RCM exacerbates this bias compared to observed.

Regional climate modelling for the southern African region is still in its infancy. There is a need for a comprehensive study of different RCM simulations over the region, similar to the US PIRCS (Project to Intercompare Regional Climate Simulations) and European PRUDENCE (Prediction of regional scenarios and uncertainties for defining European climate change risks and effects) initiatives. However, expertise in using RCMs in Africa is growing, and an AIACC (Assessments of Impacts and Adaptations to Climate Change) project for the development of regional climate change scenarios for sub-Saharan Africa has recently been funded and should provide some interesting results. This project is to be conducted by a consortium of investigators from various southern African countries, and plans to use three different RCMs (including the Hadley Centre RCM) as well as statistical methods to derive the climate change scenarios.

ACKNOWLEDGEMENTS

This study was carried out under the UK's Department for Environment, Food and Rural Affairs (DEFRA) Climate Prediction Programme (PECD 7/12/37), and the lead author was subcontracted to the Hadley Centre from the University of East Anglia (Climatic Research Unit) to perform the work. The Climate Systems Analysis Group (Department of Environmental and Geographical Science) at the University of Cape Town is thanked for access to the South African gridded precipitation data set. The lead author would also like to thank the University of Cape Town (Department of Environmental and Geographical Science) for granting her an extended period of special leave to pursue post-doctoral research in the United Kingdom.

REFERENCES

Gibson, R.K., Kallberg, P., Uppala, S., Hernandez, A., Nomura, A. and Serrano, E. 1997. ECMWF Re-Analysis Project Report Series, 1. ERA Description, ECMWF.

Giorgi, F. and Francisco, R. 2000a. Uncertainties in regional climate change predictions. A regional analysis of ensemble simulations with the HadCM2 GCM. *Climate Dynamics*, 16:169-182.

Giorgi, F. and Francisco, R. 2000b. Evaluating uncertainties in the prediction of regional climate change. *Geophysical Research Letters*, 27: 1295-1298.

Giorgi, F., Whetton, P.H., Jones, R.G., Christensen, J.H., Mearns, L.O., Hewitson, B., von Storch, H., Francisco, R. and Jack, C. 2001. Emerging patterns of simulated regional climatic changes for the 21st century due to anthropogenic forcings. *Geophysical Research Letters*, 28(17): 3317-3320.

Gordon, C., Cooper, C., Senior, C., Banks, H., Gregory, J., Johns, T., Mitchell, J. and Wood, R. 2000. The simulation of SST, sea ice extents and ocean heat transports in a coupled model without flux adjustments. *Climate Dynamics*, 16: 147-168.

Griffiths, J.F. (ed). 1972. *Climates of Africa*. World Survey of Climatology Vol 10. Elsevier, Amsterdam.

Harrison, E.F., Minnis, P., Barkstrom, B.R., Ramanathan, V. and Gibson, G.G. 1990. Seasonal variation of cloud radiative forcing derived from the Earth Radiation Budget Experiment. *Journal of Geophysical Research*, 95: 18687-18703.

Hudson, D.A. 2002. Future changes in temperature and precipitation extremes over southern Africa. DEFRA Report 2/2/02, Hadley Centre for Climate Prediction and Research, Met Office, Bracknell, U.K.

Hudson, D.A. and Jones, R.G. 2002. Simulations of present-day and future climate over southern Africa using HadAM3H. Hadley Centre Technical Note 38, Hadley Centre for Climate Prediction and Research, Met Office, Bracknell, U.K.

Hulme, M., Barrow, E.M., Arnell, N., Harrison, P.A., Downing, T.E. and Johns, T.C. 1999. Relative impacts of human-induced climate change and natural climate variability. *Nature*, 397: 688-691.

Intergovernmental Panel on Climate Change (IPCC), 1996. *Climate Change 1995 - The Science of Climate Change: Contribution of Working Group 1 to the Second Assessment Report of the Intergovernmental Panel on Climate Change*. J.T. Houghton, L.G. Meira Filho, B.A. Callander, N. Harris, A. Kattenberg and K. Maskell, (eds.), Cambridge University Press, Cambridge. 572 pp.

Intergovernmental Panel on Climate Change (IPCC), 2000. Special Report on Emissions Scenarios. Nakicenovic, N. and Swart, R. (eds.). Cambridge University Press, UK. pp 570

Intergovernmental Panel on Climate Change (IPCC), 2001. *Climate Change 2001 - The Scientific Basis: Contribution of Working Group 1 to the Third Assessment Report of the Intergovernmental Panel on Climate Change*. J.T. Houghton, Y. Ding, D.J. Griggs, M. Noguer, P.J. van der Linden, X. Dai, K. Maskell, C.A. Johnson (eds.), Cambridge University Press, Cambridge, United Kingdom and New York, NY, USA, 881pp.

Johns, T.C., Gregory, J.M., Ingram, W.J., Johnson, C.E., Jones, A., Lowe, J.A., Mitchell, J.F.B., Roberts, D.L., Sexton, D.M.H., Stevenson, D.S., Tett, S.F.B. and Woodage, M.J. 2001. Anthropogenic climate change for 1860 to 2100 simulated with the HadCM3 model under updated emissions scenarios. Hadley Centre Technical Note No. 22, Hadley Centre for Climate Prediction and Research, Met Office, Bracknell, U.K.

- Jones, R.G., Murphy, J.M. and Noguera, M. 1995. Simulation of climate change over Europe using a nested regional-climate model. I: Assessment of control climate, including sensitivity to location of lateral boundaries. *Quarterly Journal of the Royal Meteorological Society*, 121, 1413-1449.
- Jones, R.G., Murphy, J.M., Noguera, M. and Keen, A.B. 1997. Simulation of climate change over Europe using a nested regional-climate model. II: Comparison of driving and regional model responses to a doubling of carbon dioxide. *Quarterly Journal of the Royal Meteorological Society*, 123, 265-292.
- Jones, R., Hassell, D. and Murphy, J. 1999. Configuring new climate models for Europe with improved climatologies via better representation of physical processes. UKMO second year report for MERCURE, EC contract ENV4-CT97-0485.
- Jones, R., Murphy, J., Hassell, D. and Taylor, R. 2001. Ensemble mean changes in a simulation of the European climate of 2071-2100 using the new Hadley Centre regional modelling system HadAM3H/HadRM3H. DEFRA Report 2/2/01, Hadley Centre for Climate Prediction and Research, Met Office, Bracknell, U.K.
- Joubert, A.M., Katzfey, J.J., McGregor, J.L. and Nguyen, K.C. 1999. Simulating midsummer climate over southern Africa using a nested regional climate model. *Journal of Geophysical Research*, 104: 19015-19025.
- Murphy, J.M., Jones, R.G., Hassell, D.C. and Woodage, M.J. 2002. A high resolution atmospheric GCM for the generation of regional climate scenarios. (In preparation).
- New, M., Hulme M. and Jones, P. 1999. Representing twentieth-century space-time climate variability. Part I: Development of a 1961-90 mean monthly terrestrial climatology. *Journal of Climate*, 12: 829-856.
- Noguera, M., Jones, R. and Murphy, J. 1998. Sources of systematic errors in the climatology of a regional climate model over Europe. *Climate Dynamics*, 14: 691-712.
- Pope, V.D., Gallani, M.L., Rowntree, P.R. and Stratton, R.A. 2000. The impact of new physical parametrizations in the Hadley Centre climate model: HadAM3. *Climate Dynamics*, 16: 123-146.
- Rayner, N.A., Parker, D.E., Horton, E.B., Folland, C.K., Alexander, L.V., Rowell, D.P., Kent, E.C. and Kaplan, A. 2002. Global analyses of SST, sea ice and night marine air temperature since the late nineteenth century. Submitted to *Journal of Geographical Research (Atmospheres)*.
- Rossow, W.B. and Schiffer, R.A. 1991. ISCCP cloud data products. *Bulletin of the American Meteorological Society*, 72: 2-20
- Simmons, A.J. and Burridge, D.M. 1981. An energy and angular-momentum conserving finite-difference scheme and hybrid coordinates. *Monthly Weather Review*, 109:758-766.
- Sun, L., Semazzi, F.H.M., Giorgi, F. and Ogallo, L. 1999a. Application of the NCAR regional climate model to eastern Africa. 1. Simulation of the short rains of 1988. *Journal of Geophysical Research*, 104: 6529-6548.
- Sun, L., Semazzi, F.H.M., Giorgi, F. and Ogallo, L. 1999b. Application of the NCAR regional climate model to eastern Africa. 2. Simulation of interannual variability of short rains. *Journal of Geophysical Research*, 104: 6549-6562.

Taylor, R., Jones, R., Hassell, D., and Murphy, J. 2001. Analysis of errors in a new regional climate model for Europe. DETR Report 2/1/00, Hadley Centre for Climate Prediction and Research, Met Office, Bracknell, UK

Tyson, P.D. and Preston-Whyte, R.A. 2000. *The Weather and Climate of Southern Africa*. Oxford University Press, Cape Town.

Verburg, P., Kakogozo, B., Makassa, L., Muhoza, S. and Tumba, J.-M. 1998. Hydrodynamics of Lake Tanganyika: 1993-1996, Synopsis and interannual comparisons. FAO/FINNIDA Research for the Management of the fisheries on Lake Tanganyika. GCP/RAF/271/FIN-TD/87 (En & Fr): 52 pp.

Whetton, P.H., Katzfey, J.J., Hennessy, K.J., Wu, X., McGregor, J.L. and Nguyen, K. 2001. Developing scenarios of climate change for Southeastern Australia: an example using regional climate model output. *Climate Research*, 16: 181-201.

Wilson, M.F. and Hendersen-Sellers, A. 1985. A global archive of land cover and soils data for use in general circulation models. *Journal of Climatology*, 5:119-143.

Xie, P. and Arkin, P.A. 1997. Global precipitation: a 17-year monthly analysis based on gauge observations, satellite estimates and numerical model outputs. *Bulletin of the American Meteorological Society*, 78: 2539-2558.

TEMPERATURE				
	DJF	MAM	JJA	SON
Mean:				
OBS	23.72	21.66	17.93	22.51
GCM	22.11	21.08	19.01	23.78
RCM	21.93	20.77	18.74	22.86
Spatial standard deviation:				
OBS	2.10	2.73	3.94	2.70
GCM	1.87	2.51	4.15	2.82
RCM	2.32	3.00	4.26	3.11
RMS error:				
GCM	2.12	1.26	1.99	1.91
RCM	2.26	1.48	1.92	1.42
Spatial correlations:				
RCM-OBS LS	0.80	0.93	0.93	0.91
GCM-OBS LS	0.73	0.90	0.93	0.87
RCM-GCM LS	0.94	0.98	0.99	0.98
RCM-OBS MS	0.82	0.81	0.80	0.82
RCM-ORO MS	-0.86	-0.90	-0.84	-0.78
OBS-ORO MS	-0.79	-0.84	-0.84	-0.77

Table 1: Seasonal 1.5 m air temperature statistics for land points only over the RCM domain. Results show the area-averaged mean temperature and spatial standard deviation ($^{\circ}\text{C}$) for the observed (OBS) data (1961-1990 CRU climatology, New *et al.*, 1999), RCM and driving GCM, and the root-mean-square error relative to the observed data. Spatial correlations between the respective large-scale (LS) and mesoscale (MS) components are shown, including correlations with the mesoscale component of orographic height (ORO).

PRECIPITATION				
	DJF	MAM	JJA	SON
Mean:				
OBS	4.88	2.82	0.37	2.01
GCM	5.77	2.05	0.27	2.59
RCM	6.58	2.89	0.40	3.17
Spatial standard deviation:				
OBS	2.49	1.77	0.71	1.57
GCM	2.35	1.40	0.41	1.59
RCM	3.34	2.06	0.66	2.19
RMS error:				
GCM	1.87	1.36	0.33	1.01
RCM	3.01	1.53	0.57	1.77
Spatial correlations:				
RCM-OBS LS	0.81	0.78	0.68	0.86
GCM-OBS LS	0.70	0.72	0.63	0.83
RCM-GCM LS	0.87	0.92	0.91	0.95
RCM-OBS MS	0.20	0.15	0.26	0.25
RCM-ORO MS	0.40	0.26	0.05	0.33
OBS-ORO MS	0.33	0.07	-0.10	0.38

Table 2: As for Table 1, but for land precipitation (mm/day).

TEMPERATURE RESPONSE				
	DJF	MAM	JJA	SON
Mean Change:				
GCM	3.90 (3.19)	4.49 (3.00)	4.20 (3.11)	3.97 (3.26)
RCM	3.72	3.97	3.97	3.84
Spatial Standard Deviation:				
GCM	0.59	0.66	0.74	0.67
RCM	0.66	0.59	0.77	0.73
RCM MS	0.18	0.18	0.17	0.18
Spatial Correlations:				
GCM-RCM	0.90	0.88	0.95	0.95
GCM-RCM LS	0.90	0.92	0.95	0.95

Table 3: Seasonal 1.5 m air temperature response statistics for land points in the RCM domain under the A2 SRES scenario. The area-averaged mean temperature and spatial standard deviation (°C) of the response are shown, together with the spatial standard deviation of the RCM's mesoscale component (MS), and spatial correlations of the RCM and GCM response fields, and the large-scale (LS) components of these fields. The GCM numbers in brackets represent the global mean change.

PRECIPITATION RESPONSE				
	DJF	MAM	JJA	SON
Mean Change:				
GCM	-0.31 (-5.3)	-0.04 (-1.9)	-0.07 (-24.4)	-0.19 (-7.3)
RCM	-0.08 (-1.3)	0.09 (3.3)	-0.12 (-30.0)	-0.22 (-7.1)
Spatial Standard Deviation:				
GCM	0.70	0.40	0.13	0.61
RCM	0.95	0.63	0.24	0.87
RCM MS	0.46	0.29	0.11	0.31
Spatial Correlations:				
GCM-RCM	0.75	0.75	0.86	0.88
GCM-RCM LS	0.85	0.83	0.88	0.93

Table 4: As for Table 3, but for land precipitation (mm/day). The numbers in brackets indicate the percentage change in precipitation over southern Africa.

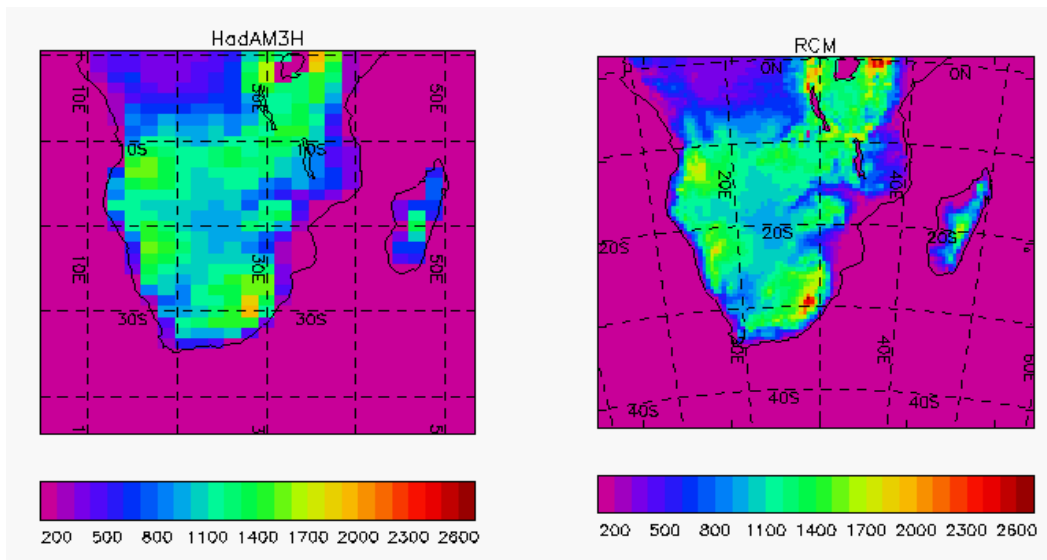


Figure 1: Distribution of orographic height (m) in the GCM (HadAM3H) and RCM.

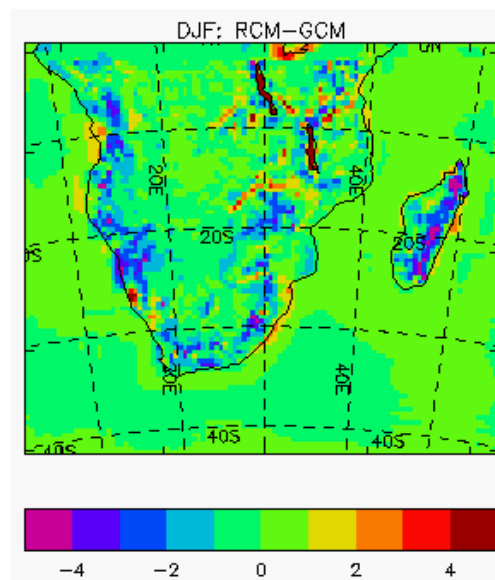


Figure 2: 30-year mean difference between the 1.5 m temperature ($^{\circ}\text{C}$) simulated by the RCM and the driving GCM (HadAM3H) for December to February (DJF).

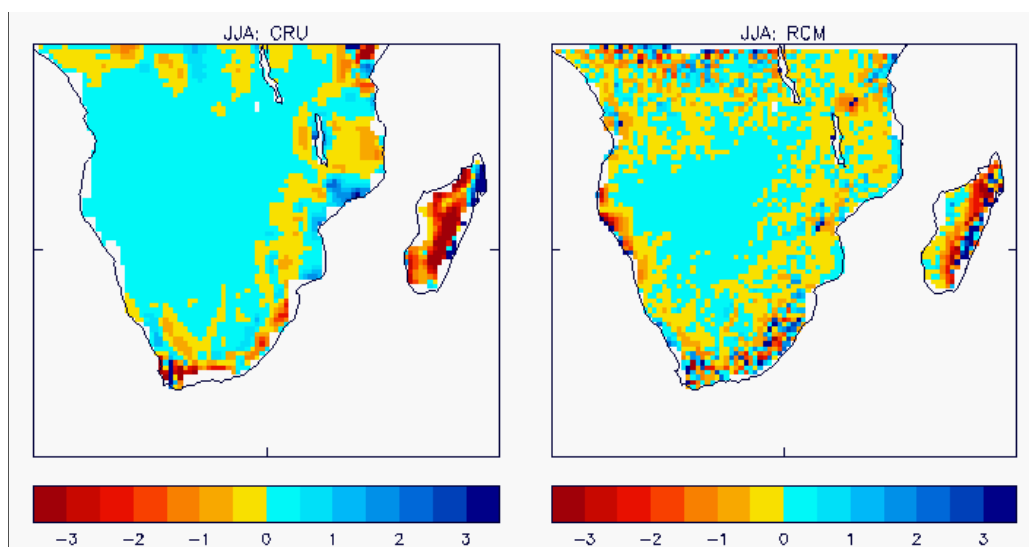


Figure 3: The standardised (z-scores) mesoscale component of precipitation from the CRU observed data (New *et al.*, 1999) and RCM in winter (JJA).

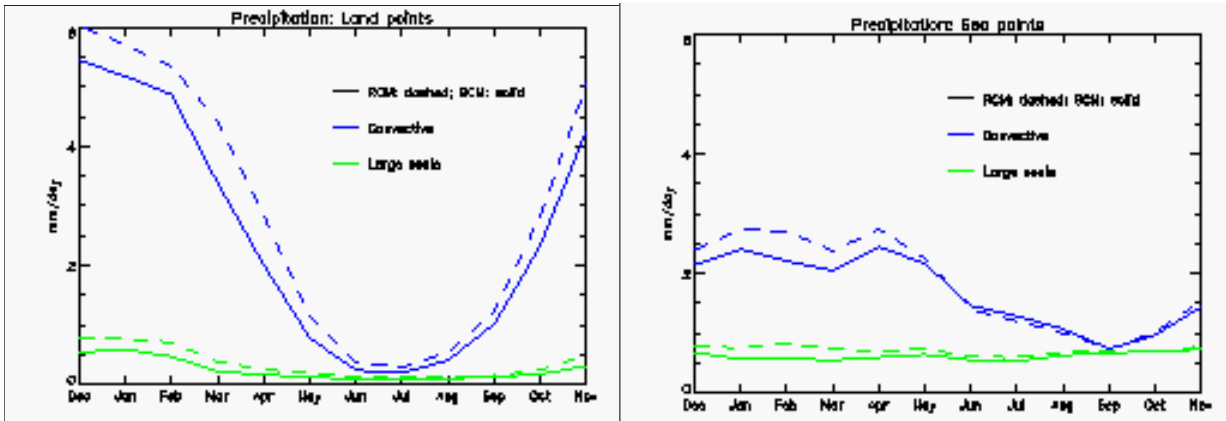


Figure 4: Seasonal cycle of convective and large-scale precipitation (mm/day) averaged over 30-year control integrations of the RCM (dashed) and driving GCM (solid) over land points (left) and sea points (right) in the RCM domain (4-point buffer zone removed).

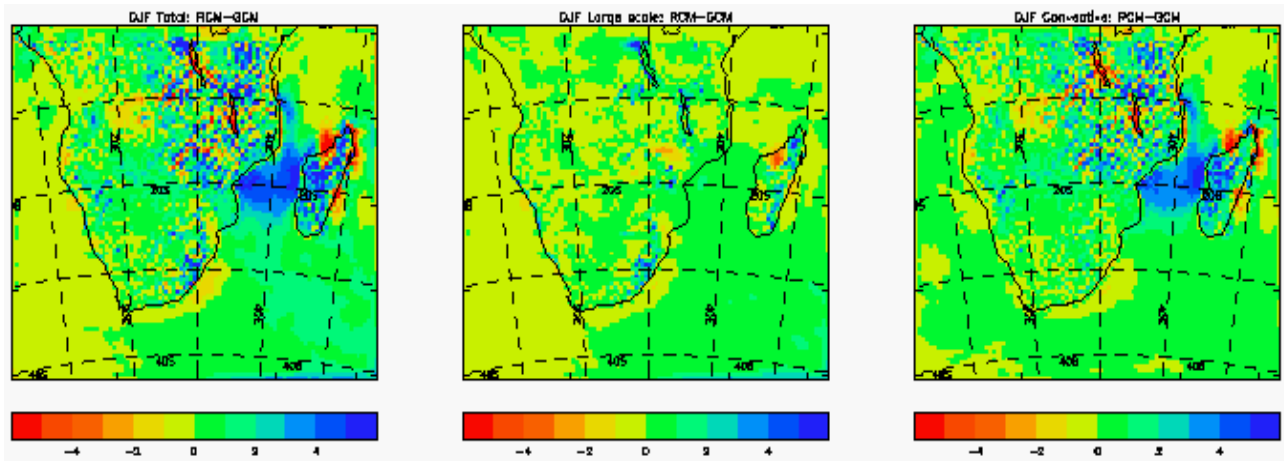


Figure 5: 30-year mean difference between total, large scale and convective precipitation (mm/day) simulated by the RCM and the driving GCM (HadAM3H) for December to February (DJF).

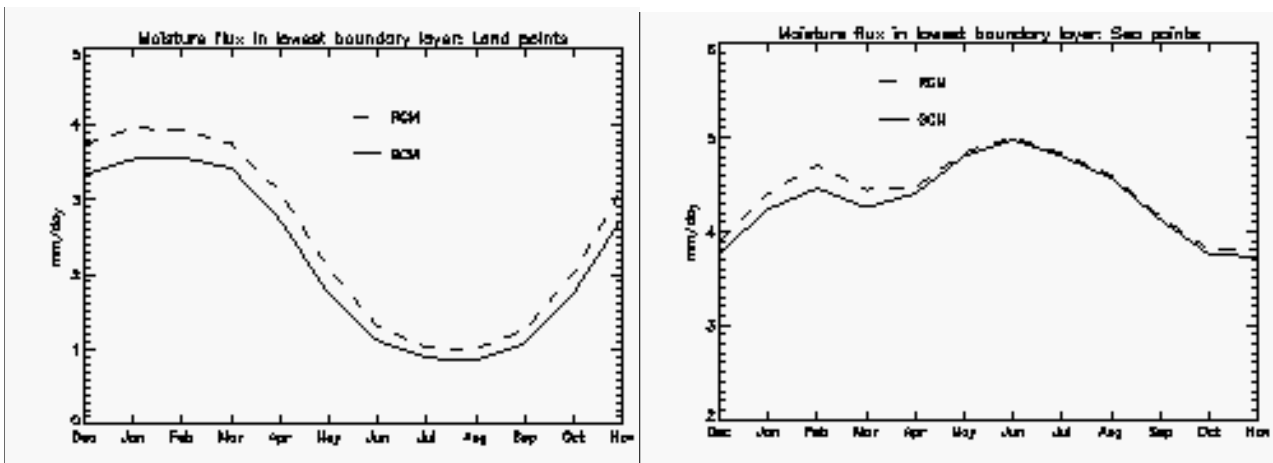


Figure 6: Seasonal cycle of the surface total moisture flux (mm/day), averaged over 30-year control integrations of the RCM (dashed) and driving GCM (solid) over land points (left) and sea points (right) in the RCM domain (4-point buffer zone removed).

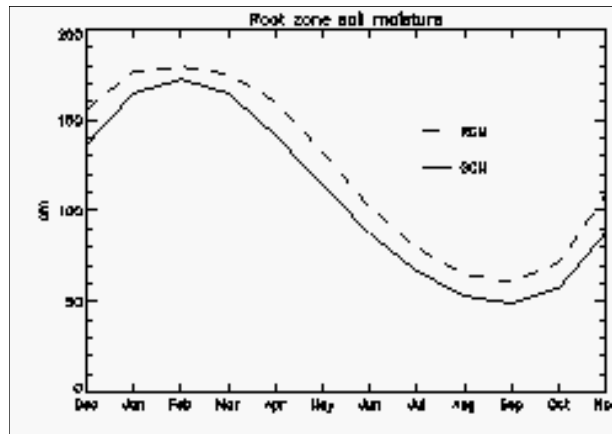


Figure 7: Seasonal cycle of the soil moisture content (cm) averaged over 30-year control integrations of the RCM (dashed) and driving GCM (solid) in the RCM domain (4-point buffer zone removed).

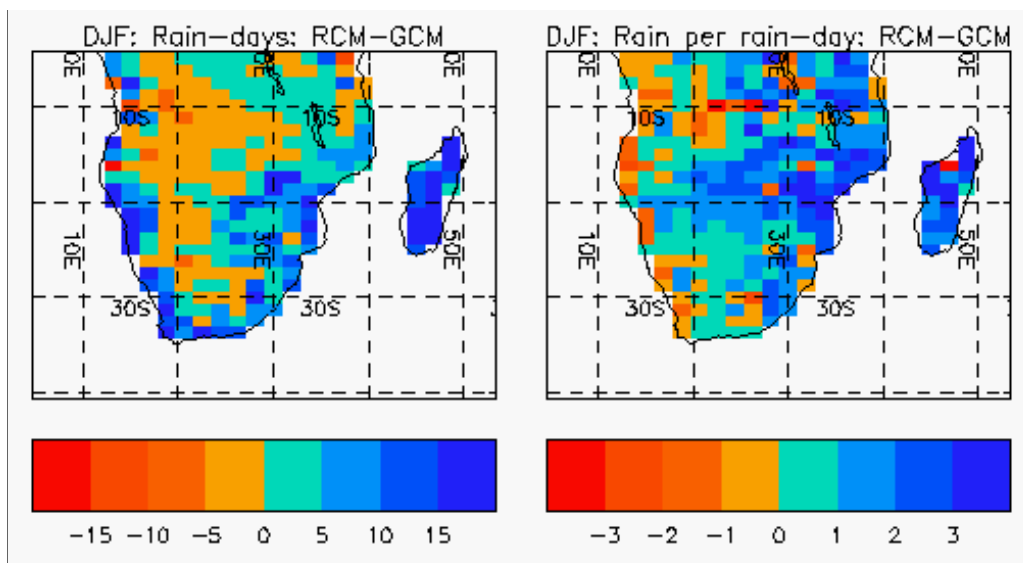


Figure 8: 30-year mean difference between the average number of rain-days (a rain-day is defined as having more than 0.2 mm of rain) (left) and the rain per rain-day (mm) (right) simulated by the RCM (daily data are aggregated to the GCM-scale) and the driving GCM (HadAM3H) for December to February (DJF).

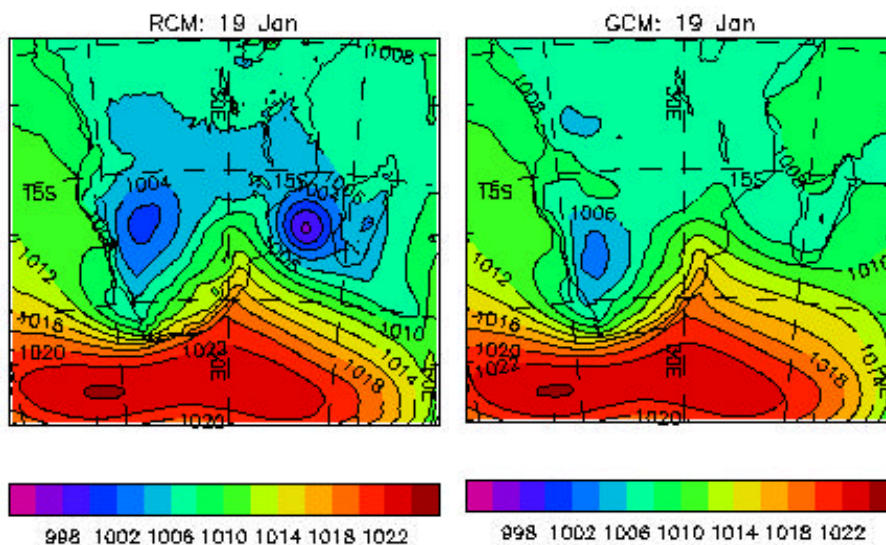


Figure 9: A tropical cyclone is evident in the mean sea-level pressure (hPa) field from the RCM but not in the driving GCM for the corresponding day.

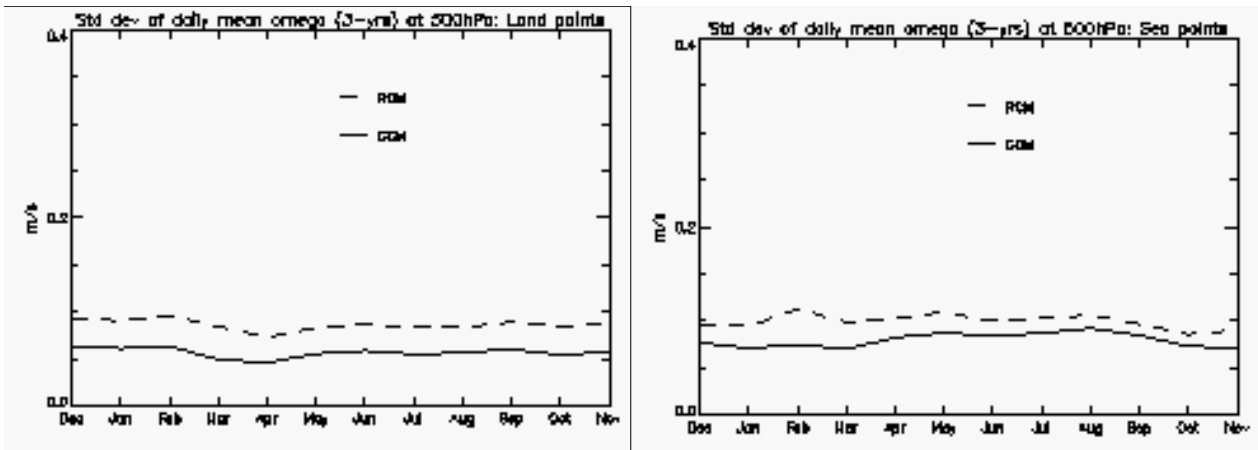


Figure 10: Seasonal cycle of the standard deviation of daily mean vertical velocity (m/s) at 500 hPa in the RCM (dashed) and driving GCM (solid) over land points (left) and sea points (right) in the RCM domain (4-point buffer zone removed). The results are based on 3 years of data.

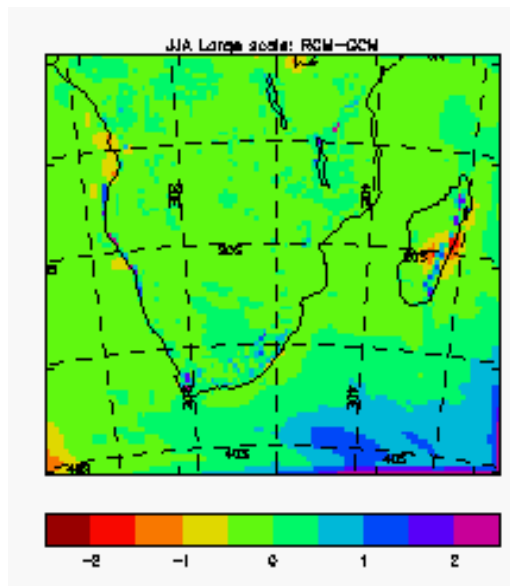


Figure 11: 30-year mean difference between large scale precipitation (mm/day) simulated by the RCM and the driving GCM (HadAM3H) for June to August (JJA).

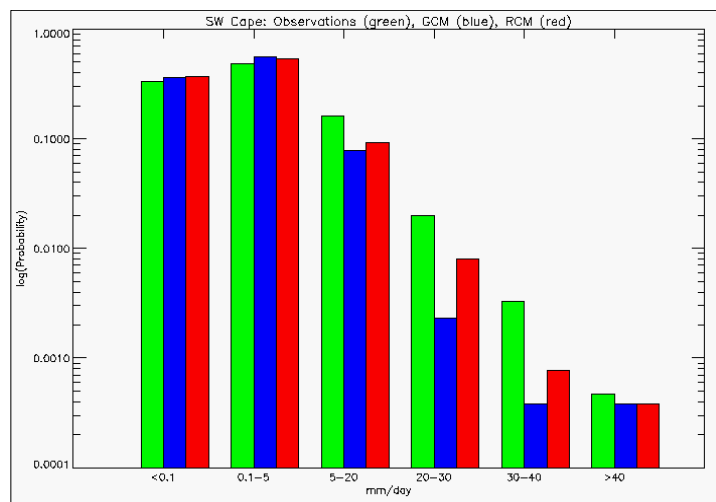


Figure 12: The probability of different amounts of daily precipitation for the South Western Cape in winter from observations (CCWR data, see Hudson and Jones, 2002), the driving GCM and the RCM.

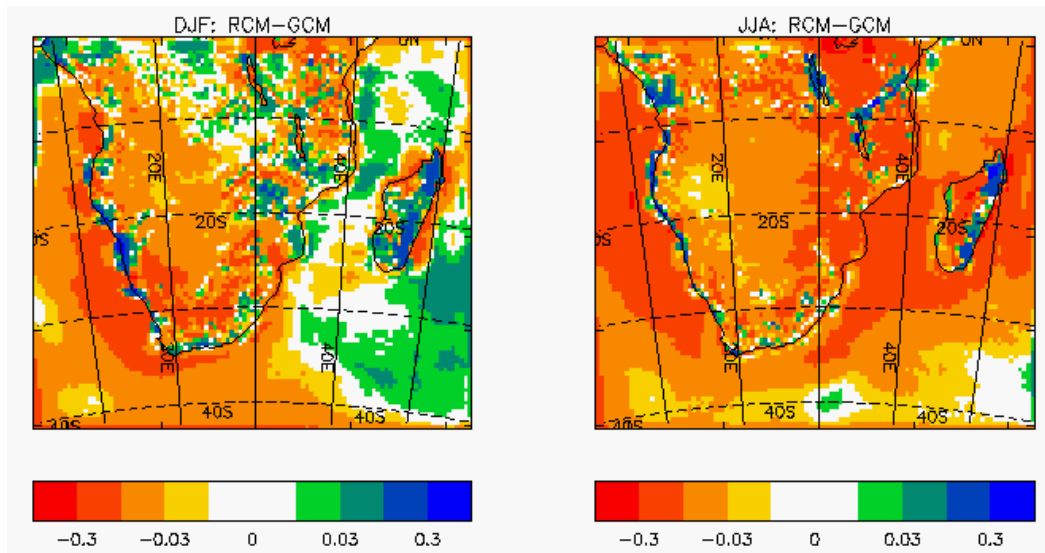


Figure 13: 30-year mean difference between the total cloud fraction simulated by the RCM and the driving GCM (HadAM3H) for December to February (DJF) and June to August (JJA).

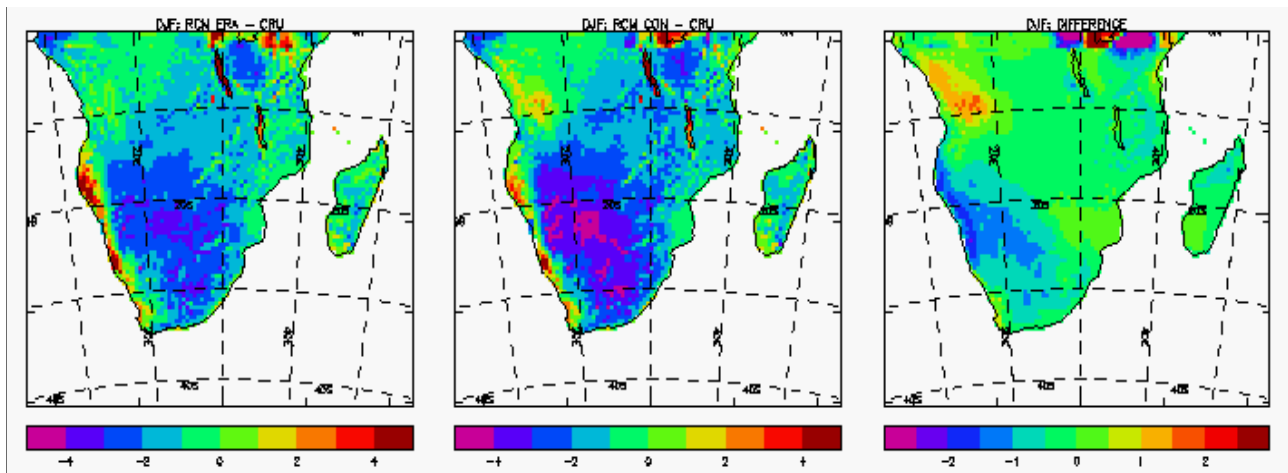


Figure 14: 1.5 m temperature ($^{\circ}\text{C}$) errors in RCM ERA (left) and RCM CON (middle) relative to the CRU climatology (1961-1990) (New *et al.*, 1999) for December to February (DJF). The right panel shows the difference between these two errors.

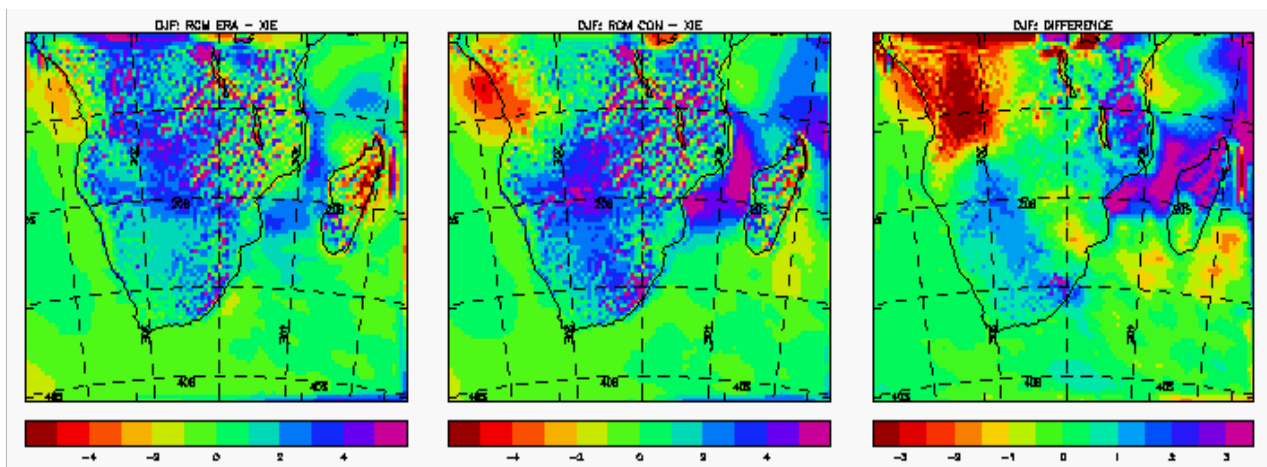


Figure 15: Total precipitation (mm/day) errors in RCM ERA (left) and RCM CON (middle) relative to the CMAP data (1979-1999) (Xie and Arkin, 1997) for December to February (DJF). The right panel shows the difference between these two errors.

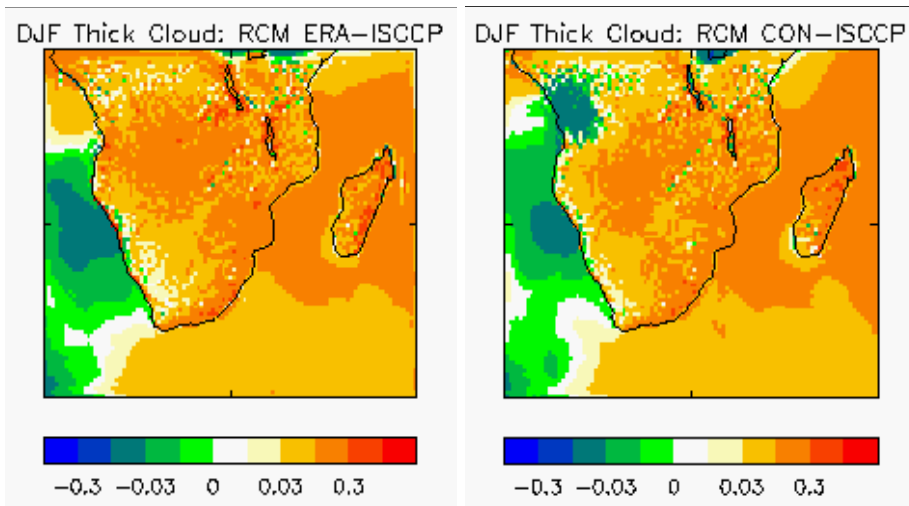


Figure 16: Thick cloud fraction errors in RCM ERA (left) and RCM CON (right) relative to the ISCCP data (1989-1993) (Rossow and Shiffer, 1991) for December to February (DJF).

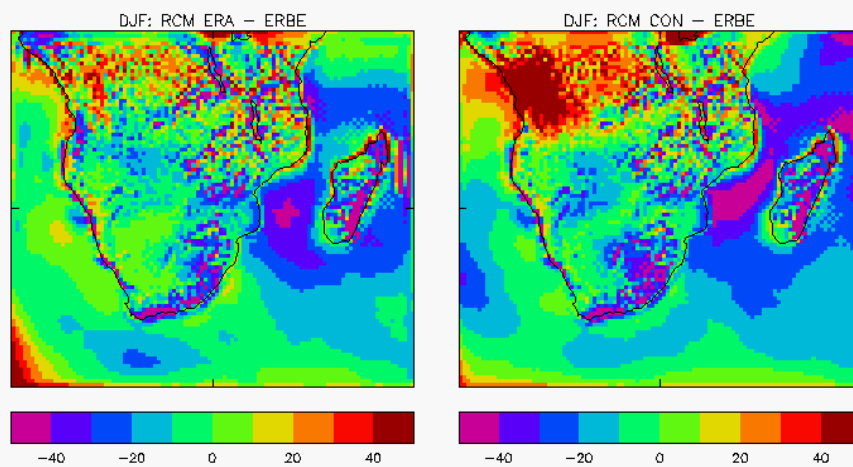


Figure 17: Shortwave cloud forcing errors in RCM ERA (left) and RCM CON (right) relative to the ERBE data (1985-1990) (Harrison *et al.*, 1990) for December to February (DJF). Negative values indicate greater shortwave cloud forcing (i.e. more outgoing shortwave radiation)

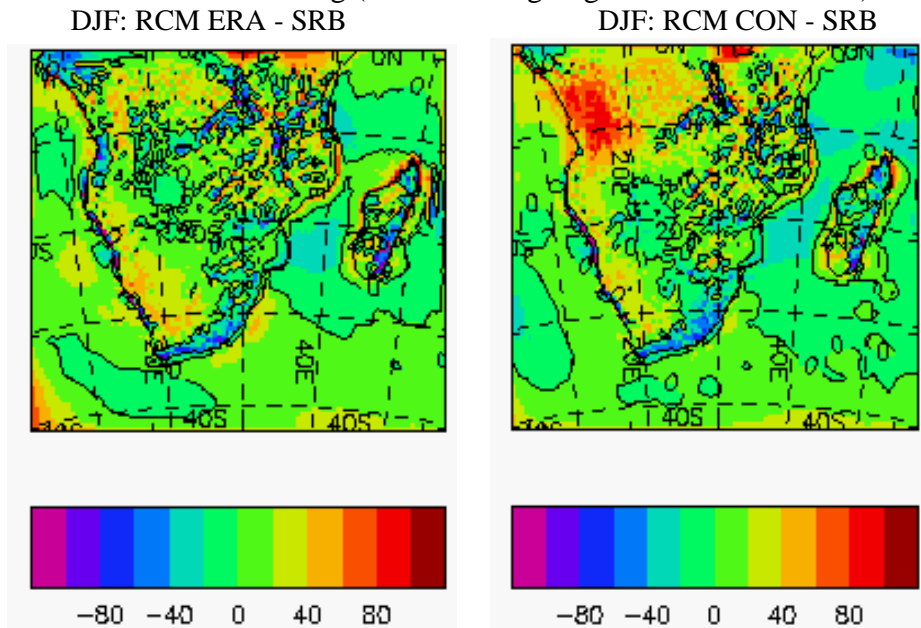


Figure 18: Bias in insolation reaching the surface (shortwave down; W/m^2) in RCM ERA (left) and RCM CON (right) relative to the Surface Radiation Balance data (1983-1991) (http://charm.larc.nasa.gov/GUIDE/campaign_documents/srb_project.html; http://charm.larc.nasa.gov/GUIDE/dataset_documents/srb.html) for December to February (DJF).

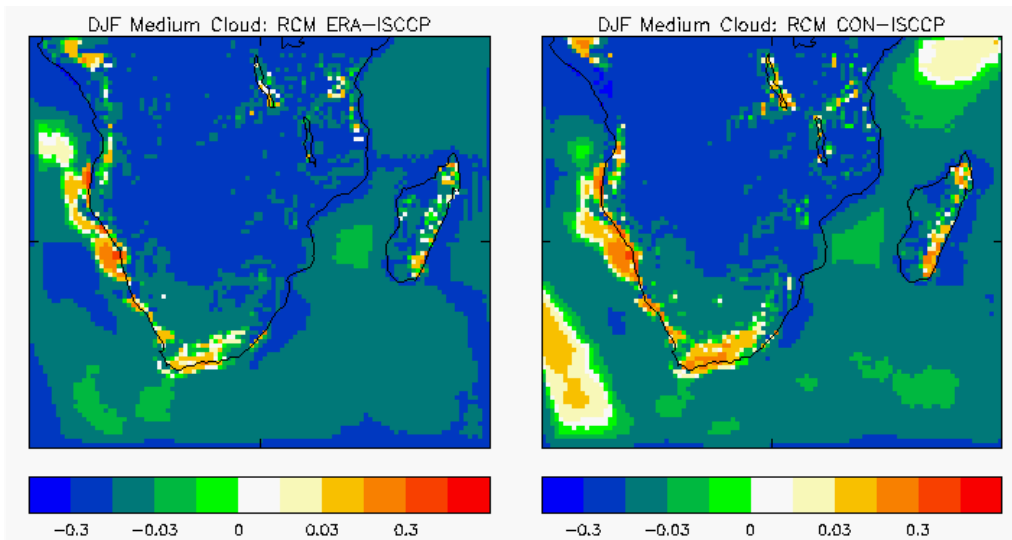


Figure 19: Medium cloud fraction errors in RCM ERA (left) and RCM CON (right) relative to the ISCCP data (1989-1993) (Rossow and Shiffer, 1991) for December to February (DJF).

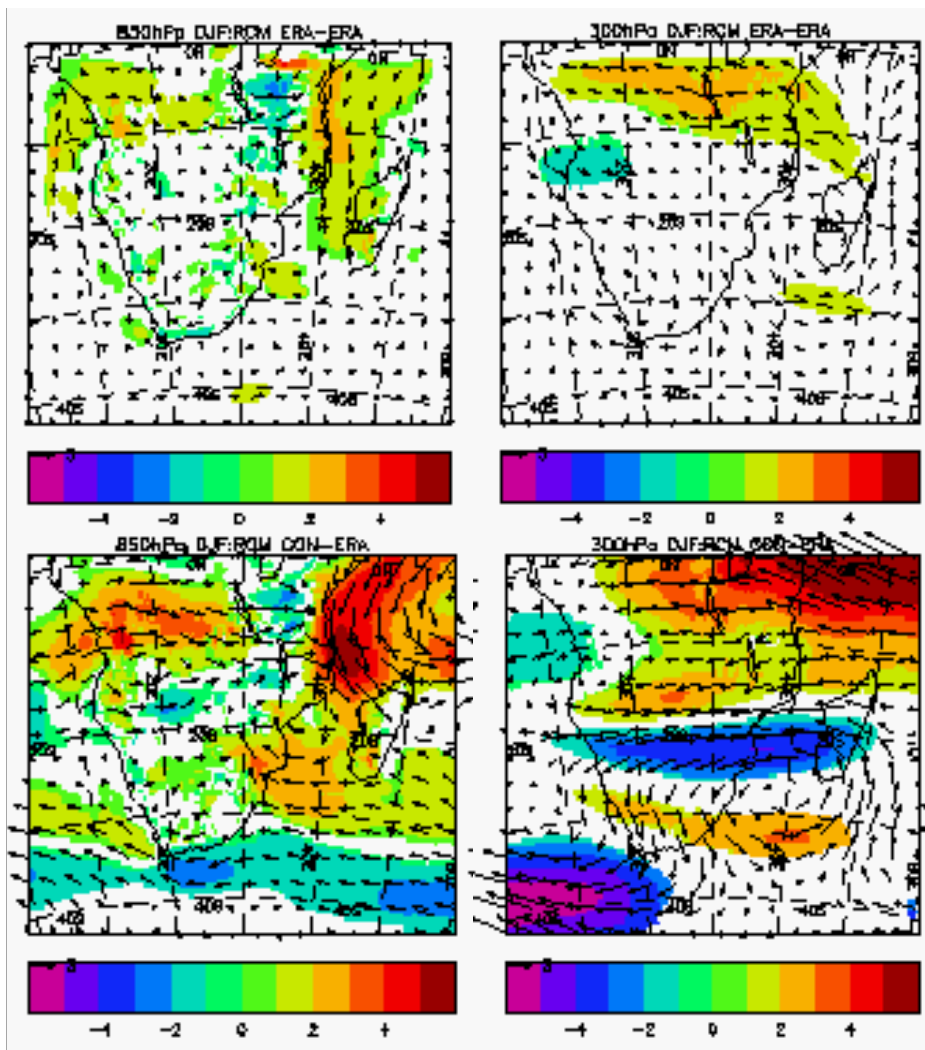


Figure 20: Wind speed (m/s) and direction errors in RCM ERA (top) and RCM CON (bottom) at the 850 hPa (left) and 300 hPa (right) levels relative to ERA reanalysis data (1979-1993) (Gibson *et al.*, 1997) for December to February (DJF). Positive and negative wind speed anomalies which are significantly different (1% level) from the ERA reanalysis data are shaded.

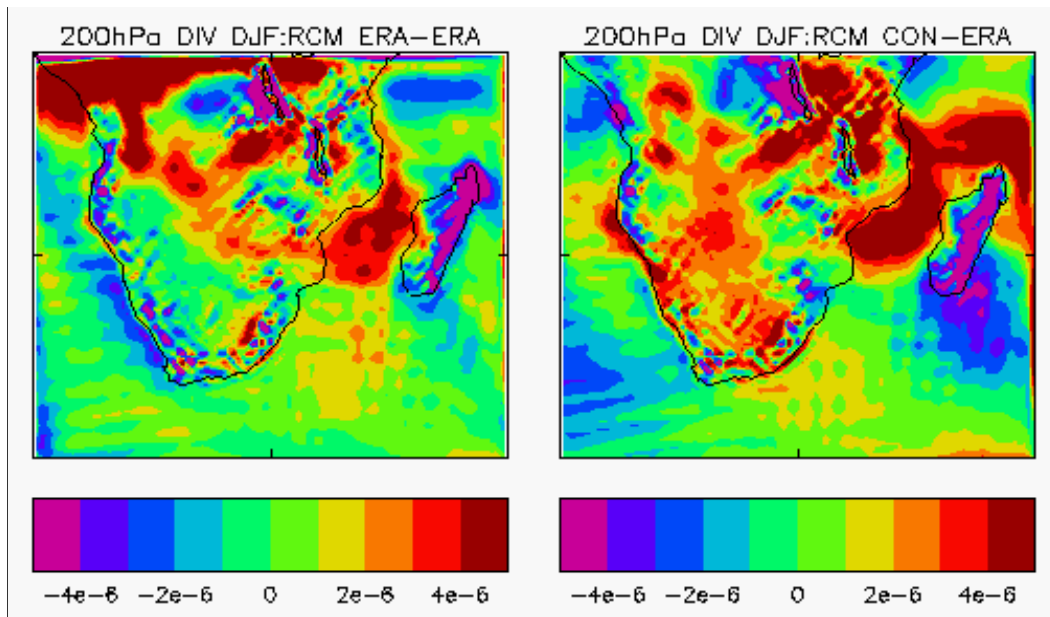


Figure 21: Horizontal divergence (s^{-1}) errors at the 200 hPa level in RCM ERA (left) and RCM CON (right) relative to ERA reanalysis data (1979-1993) (Gibson *et al.*, 1997) for December to February (DJF).

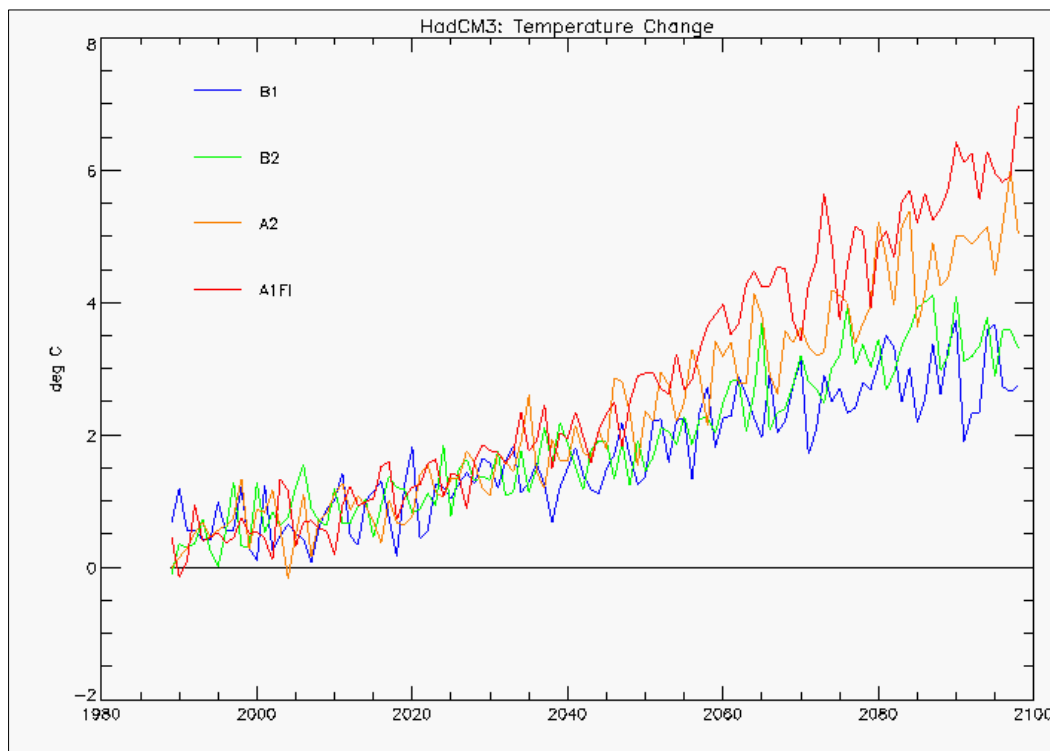


Figure 22: Area-averaged 1.5 m temperature change over land points in the southern African RCM domain from HadCM3 (fully coupled ocean-atmosphere GCM) under the B1, B2, A2 and A1FI SRES (IPCC, 2000) emissions scenarios.

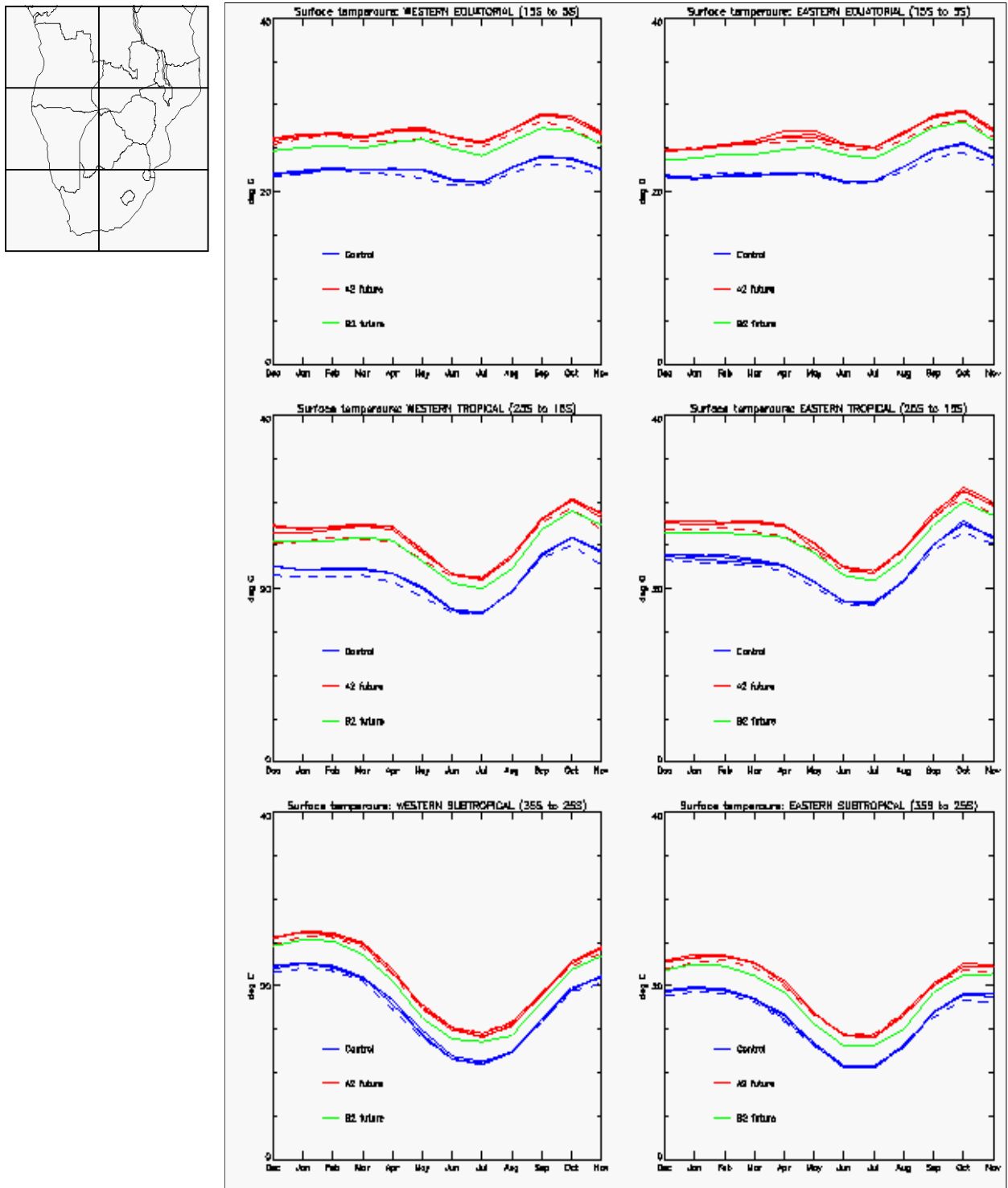


Figure 23: Seasonal cycle of the 30-year mean 1.5 m temperature (°C) for the control and SRES A2 and B2 scenario simulations from the GCM (solid lines), and the control and A2 simulation from the RCM (dashed lines). The results are area averaged over 6 land regions of southern Africa with 24°E as the diving meridian (as shown on the inset).

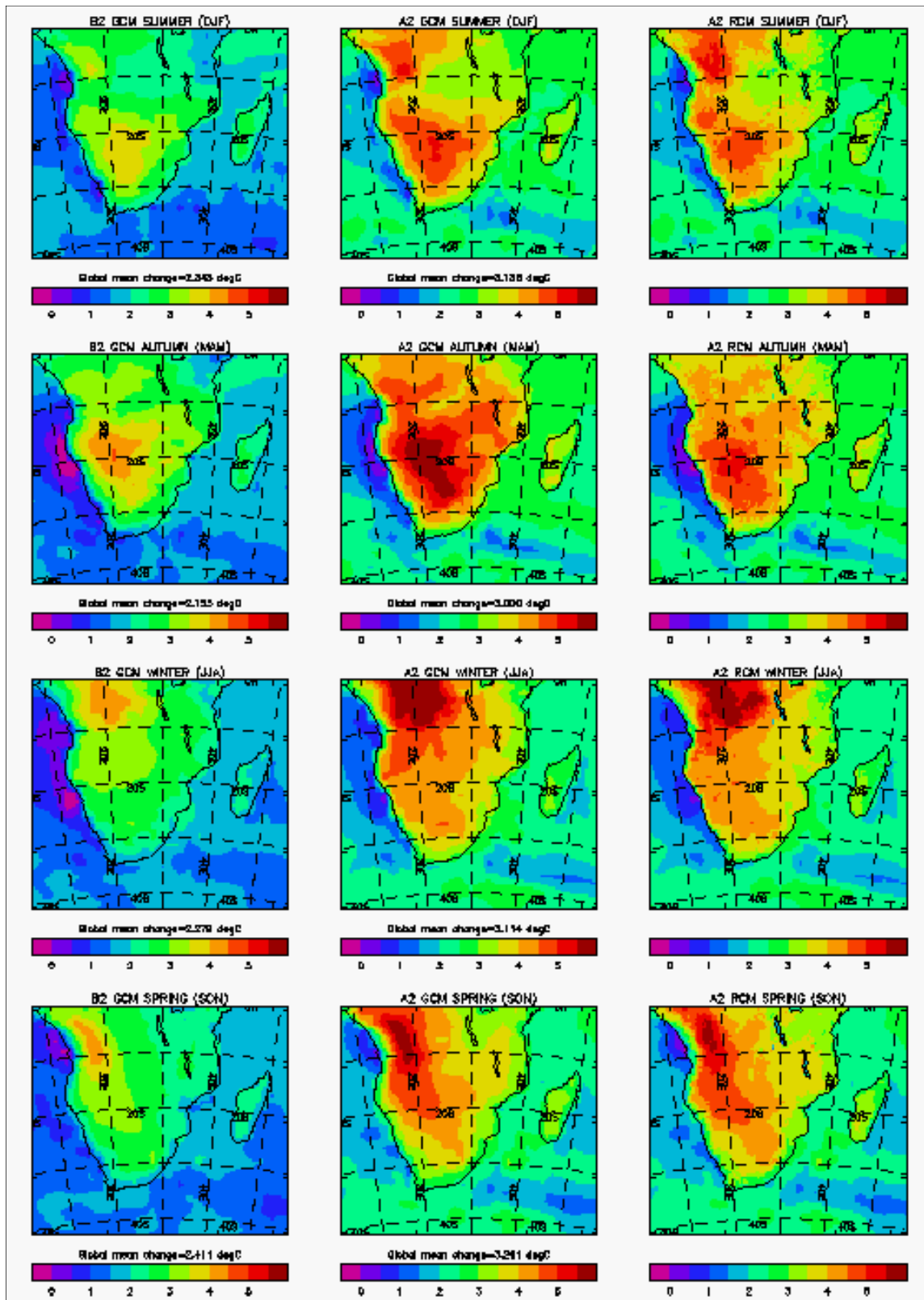


Figure 24: 30-year seasonal mean changes in 1.5 m temperature ($^{\circ}\text{C}$) from the GCM under the B2 (left) and A2 scenarios (middle) and the RCM for the A2 scenario (right) for the 2080s relative to the present-day. The GCM A2 results are based on the simulation that forces the RCM and not the ensemble mean.

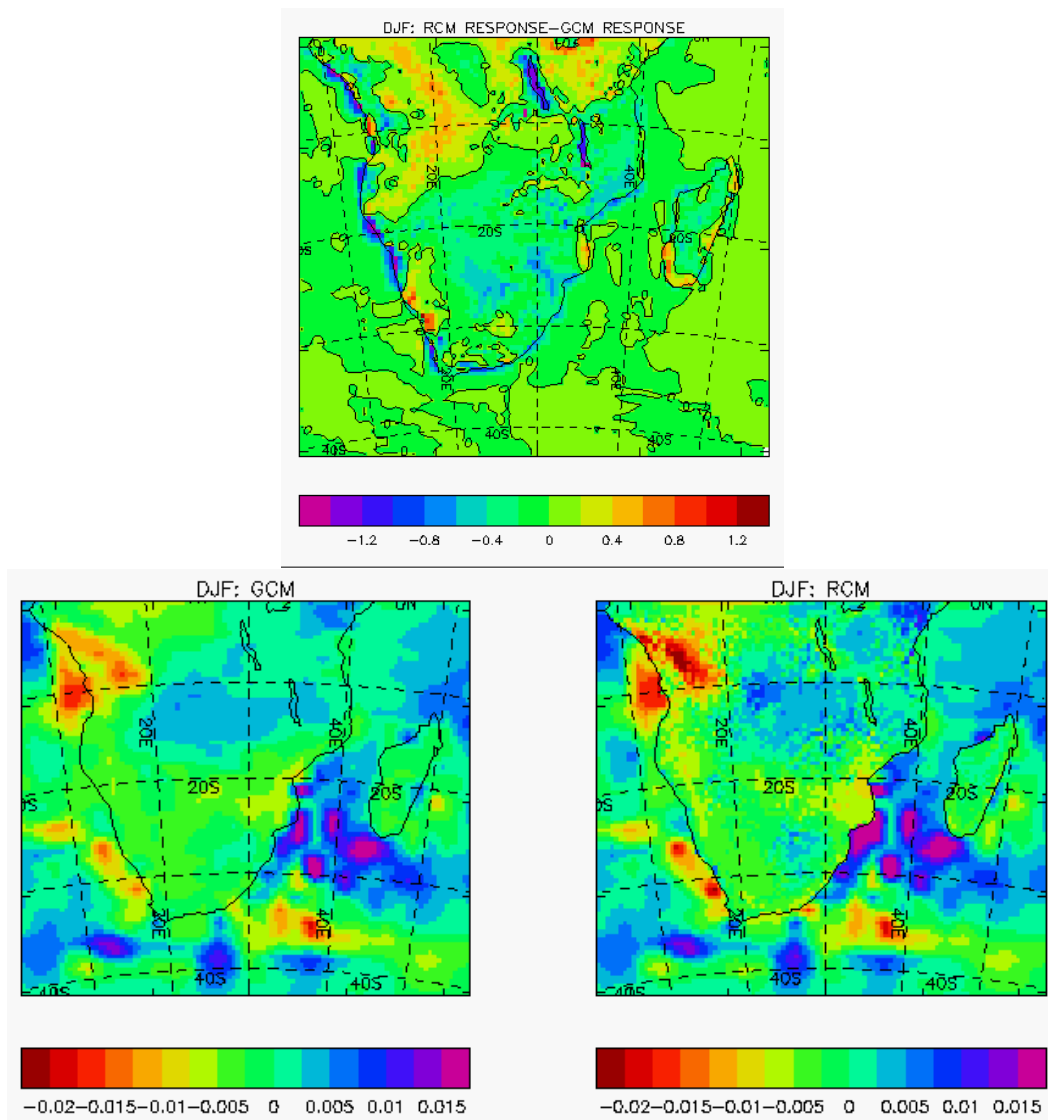


Figure 25: 30-year mean difference between the RCM and GCM 1.5m temperature ($^{\circ}\text{C}$) response to climate change for the 2080s relative to the present-day under the A2 scenario in summer (top), and the surface total moisture flux ($\text{g}/\text{m}^2/\text{s}$) response from the GCM (bottom left) and RCM (bottom right) under the A2 emissions scenario.

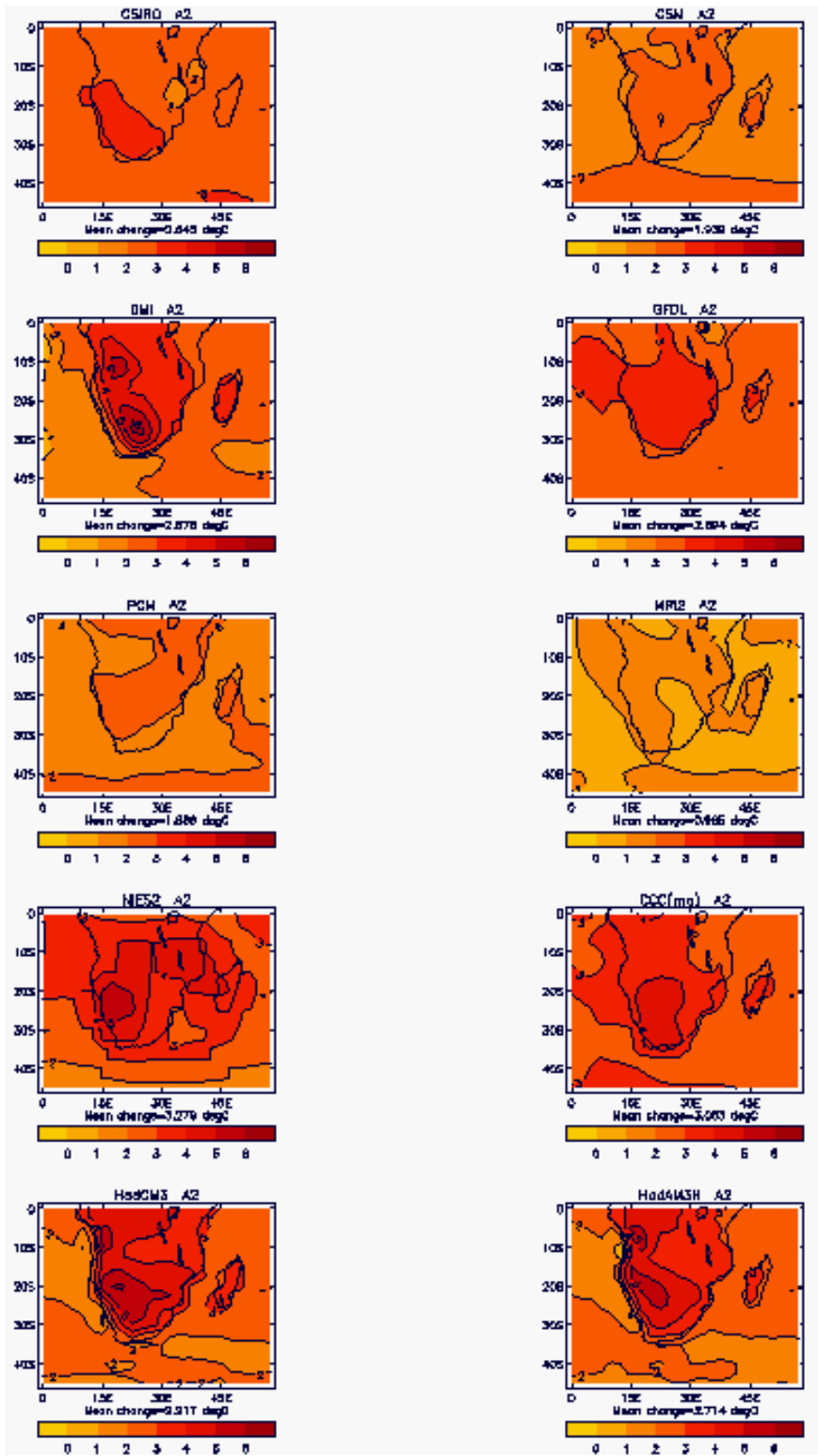


Figure 26: 30-year mean change in summer (DJF) surface air temperature ($^{\circ}\text{C}$) for the 2080s relative to the present-day under the A2 emissions scenario for a number of different GCMs. The mean change underneath each panel refers to the area averaged change over the domain shown. The GCMs are the same as those used by Giorgi *et al.* (2001), except for HadAM3H, shown in this figure. [CSIRO: Commonwealth Scientific and Industrial Research Organisation's Mk2 model (Australia); CSM: Climate System Model, National Centre for Atmospheric Research (USA); DMI: Max-Planck Institute for Meteorology (Germany) and Danish Meteorological Institute's ECHAM4-OPYC model; GFDL: Geophysical Fluid Dynamical Laboratory's R30-C model; PCM: Department of Energy (USA) and the National Centre for Atmospheric Research's Parallel Climate Model; MRI2: Meteorological Research Institute's (Japan) GCM (V2); NIES2: Centre for Climate Study Research (Japan) and National Institute for Environmental Studies' (Japan) GCM (V2); CCC(ma): Canadian Center for Climate (Modelling and Analysis) CGCM2 model; HadCM3: Hadley Centre GCM; HadAM3H: Hadley Centre's high resolution atmosphere-only GCM.]

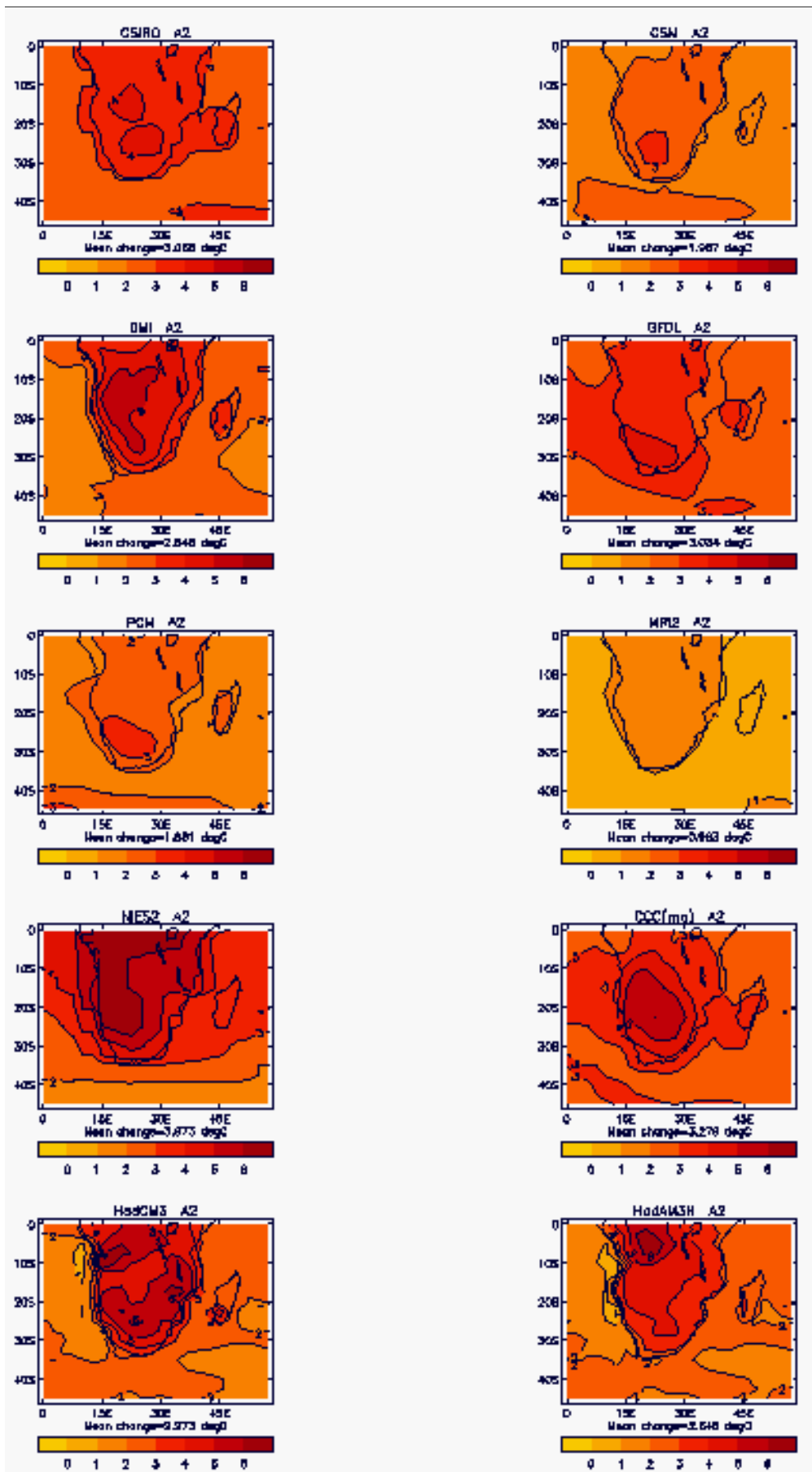


Figure 27: As for Figure 26, but for winter (JJA).

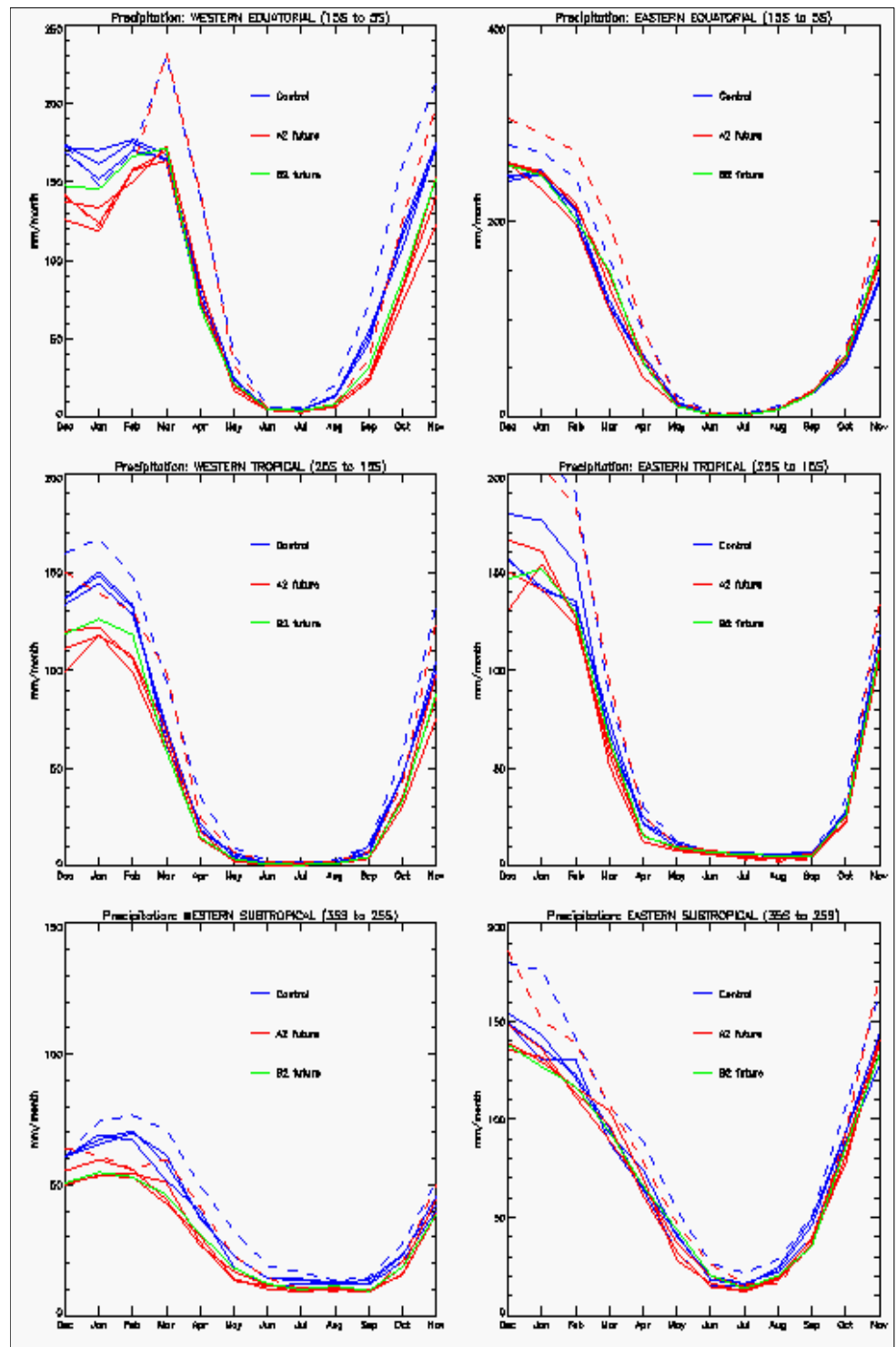
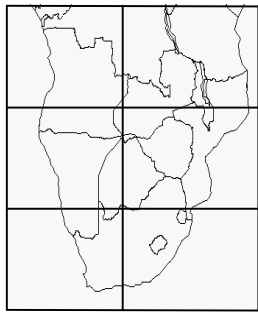


Figure 28: Seasonal cycle of the 30-year mean precipitation (mm/day) for the control and SRES A2 and B2 scenario simulations from the GCM (solid lines), and the control and A2 simulation from the RCM (dashed lines), area averaged over 6 land regions of southern Africa with 24°E as the diving meridian (as shown on the inset).

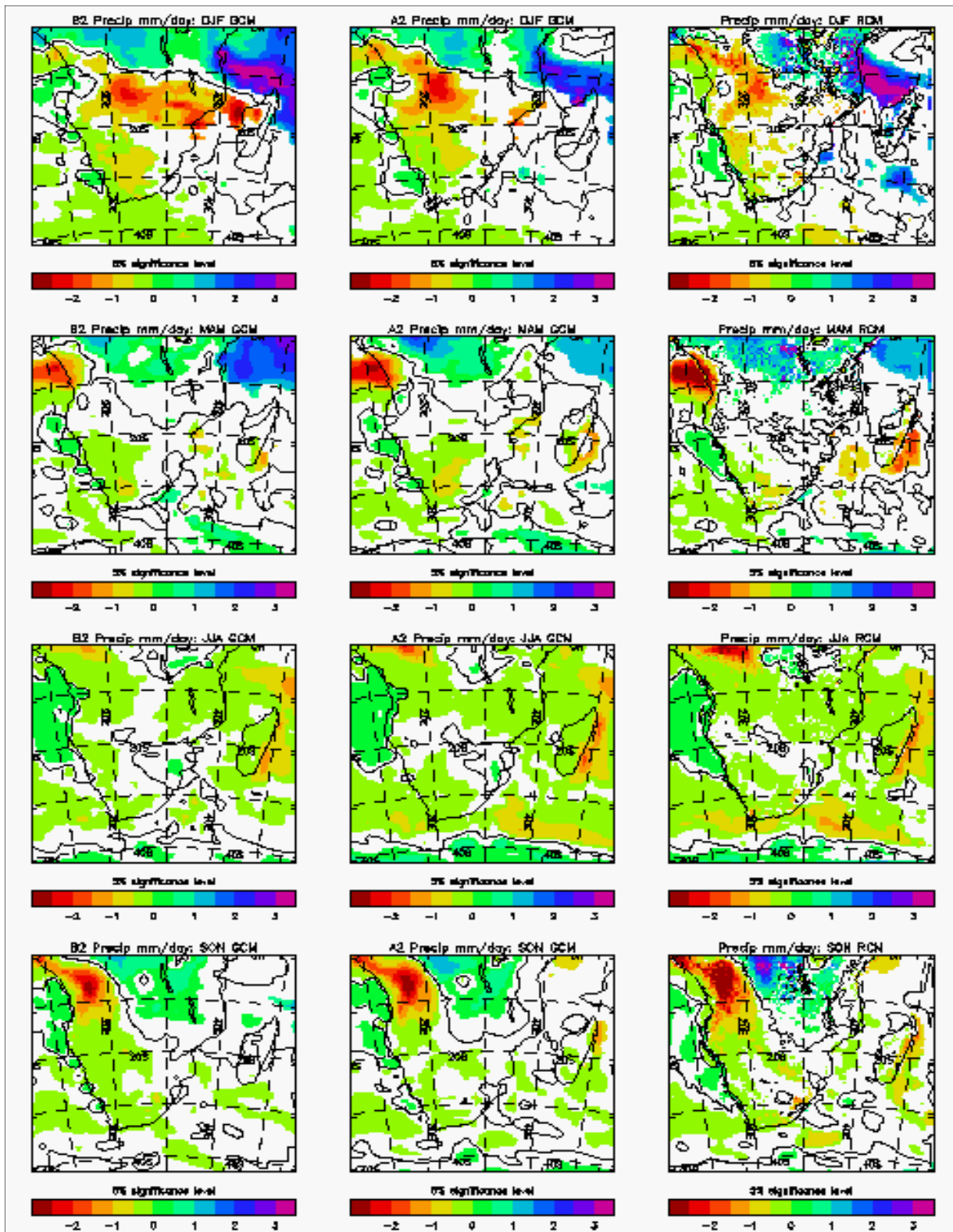


Figure 29: 30-year seasonal mean changes in precipitation (mm/day) from the GCM under the B2 (left) and A2 scenarios (middle) and the RCM for the A2 scenario (right) for the 2080s relative to the present-day. The GCM A2 results are based on the simulation that forces the RCM and not the ensemble mean. Changes significant at the 5% significance level (t-test) are shaded and the zero contour line is drawn.

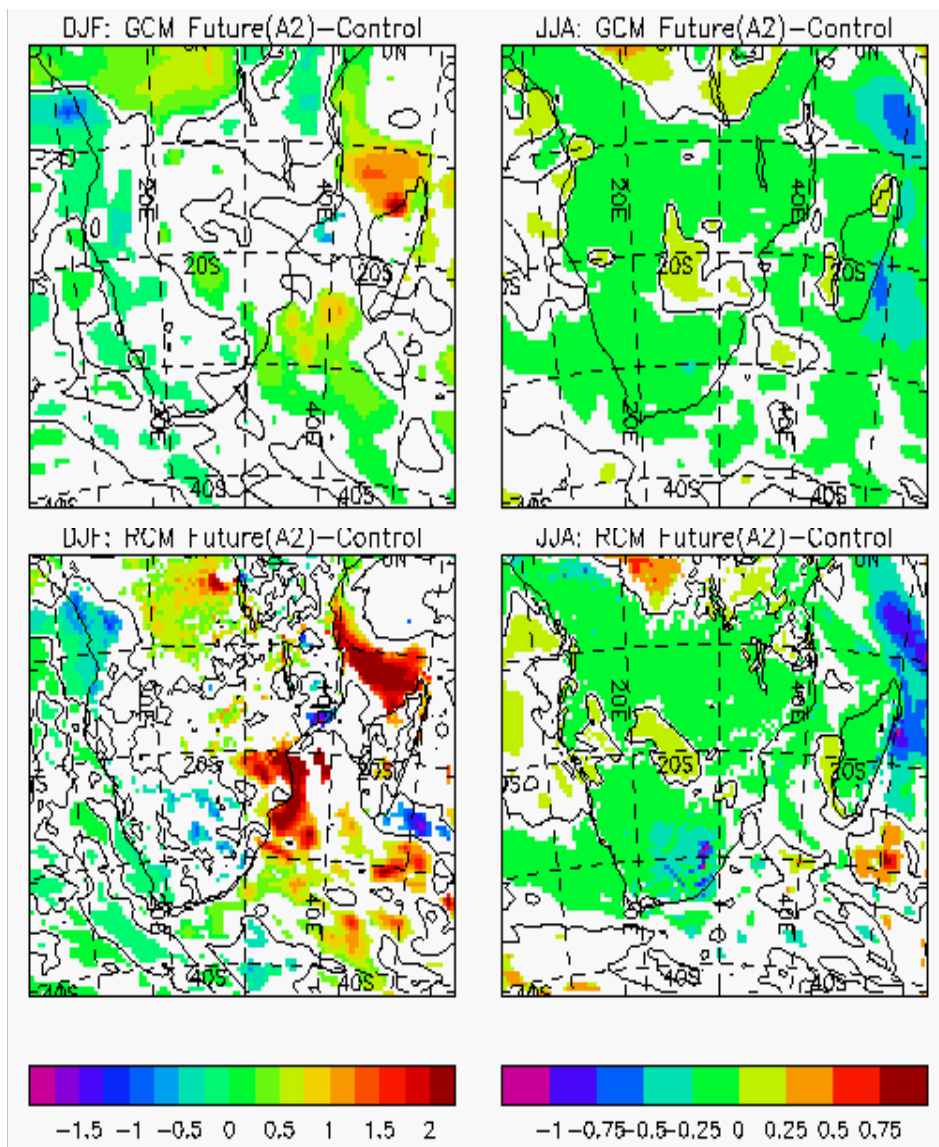


Figure 30: 30-year mean difference between the interannual variability of seasonal mean precipitation (mm/day) simulated by the SRES A2 scenario (2080s) and control simulations for December to February (DJF) and June to August (JJA) in the GCM (top) and RCM (bottom). Changes significant at the 5% significance level (F-test) are shaded and the zero contour line is drawn.

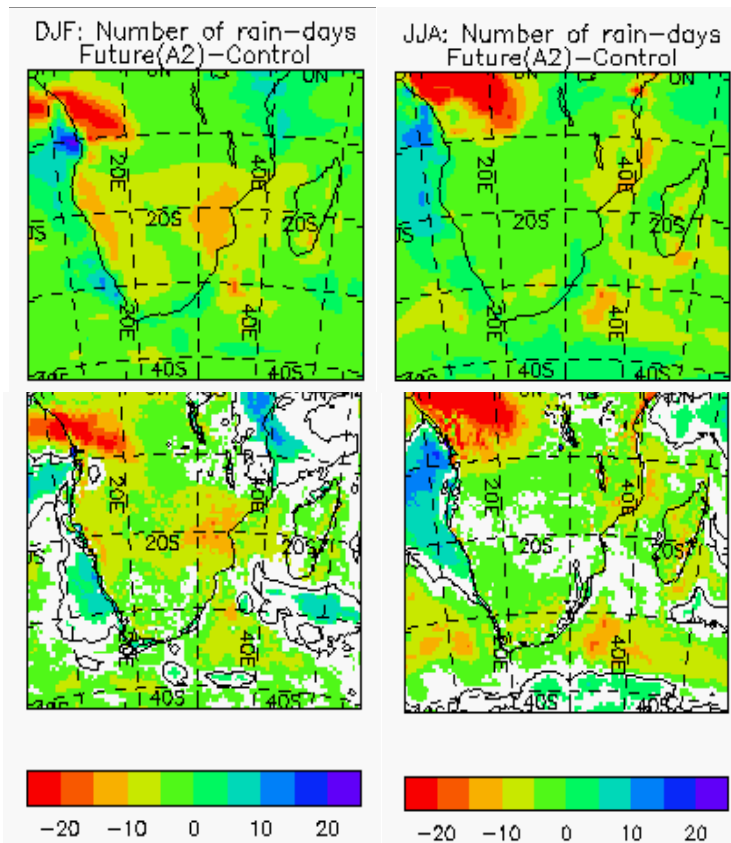


Figure 31: 30-year mean difference between the average number of rain-days (days with more than 0.2mm of rain) between the SRES A2 scenario (2080s) and control simulations for December to February (DJF) (left) and June to August (JJA) (right) from the driving GCM (top panel) and the RCM (bottom panel). Positive and negative changes in RCM that are significant at the 5% significance level (t-test) are shaded and the zero contour line is drawn.

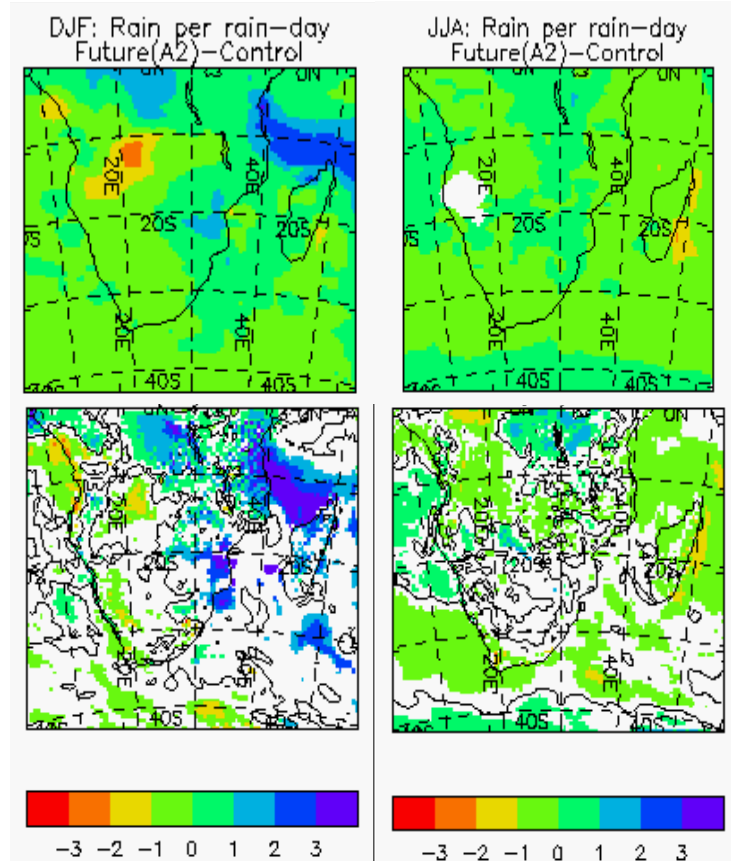


Figure 32: As for Figure 31, but for rainfall intensity (mm/day).

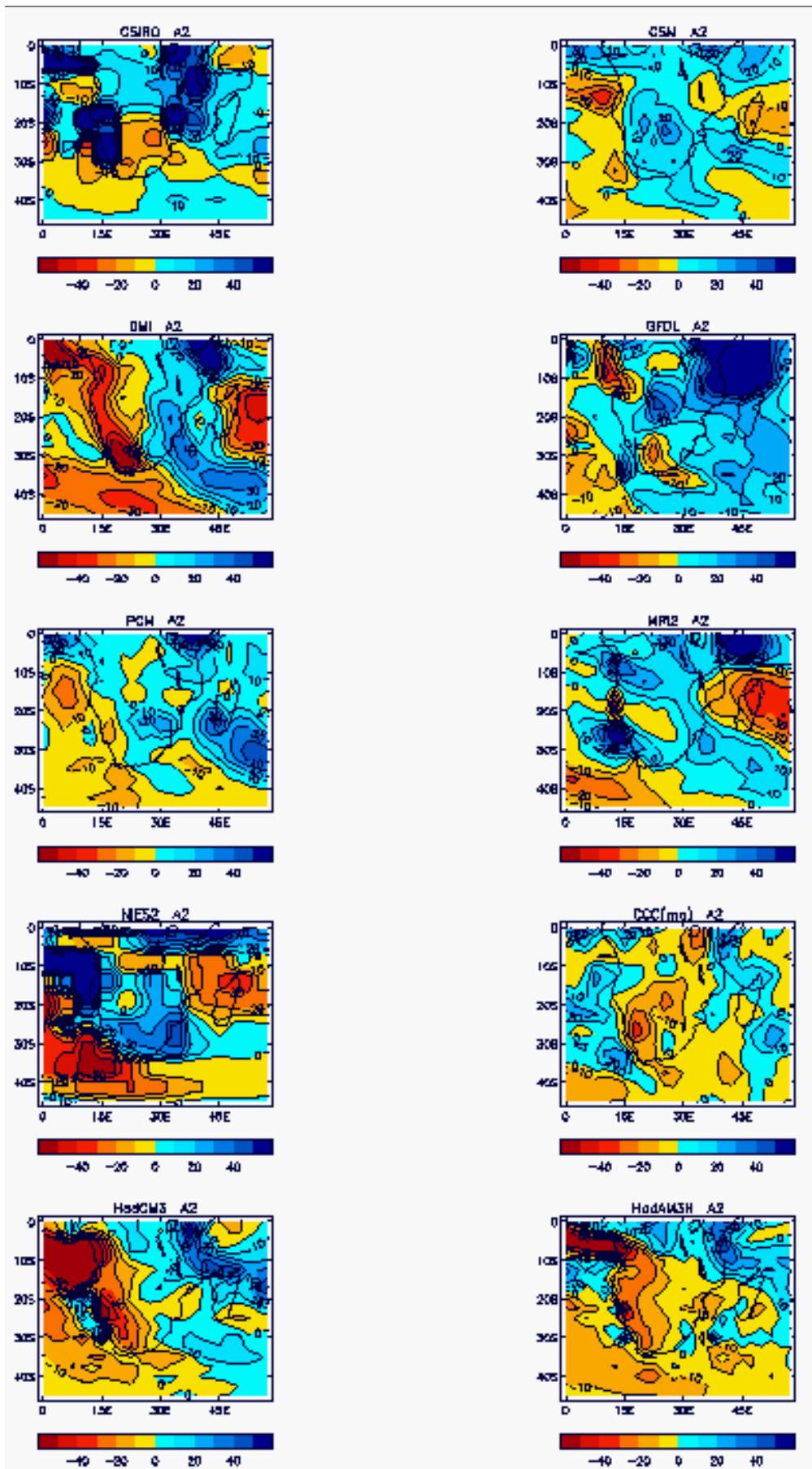


Figure 33: As for Figure 26, but for precipitation (% change) in summer (DJF).

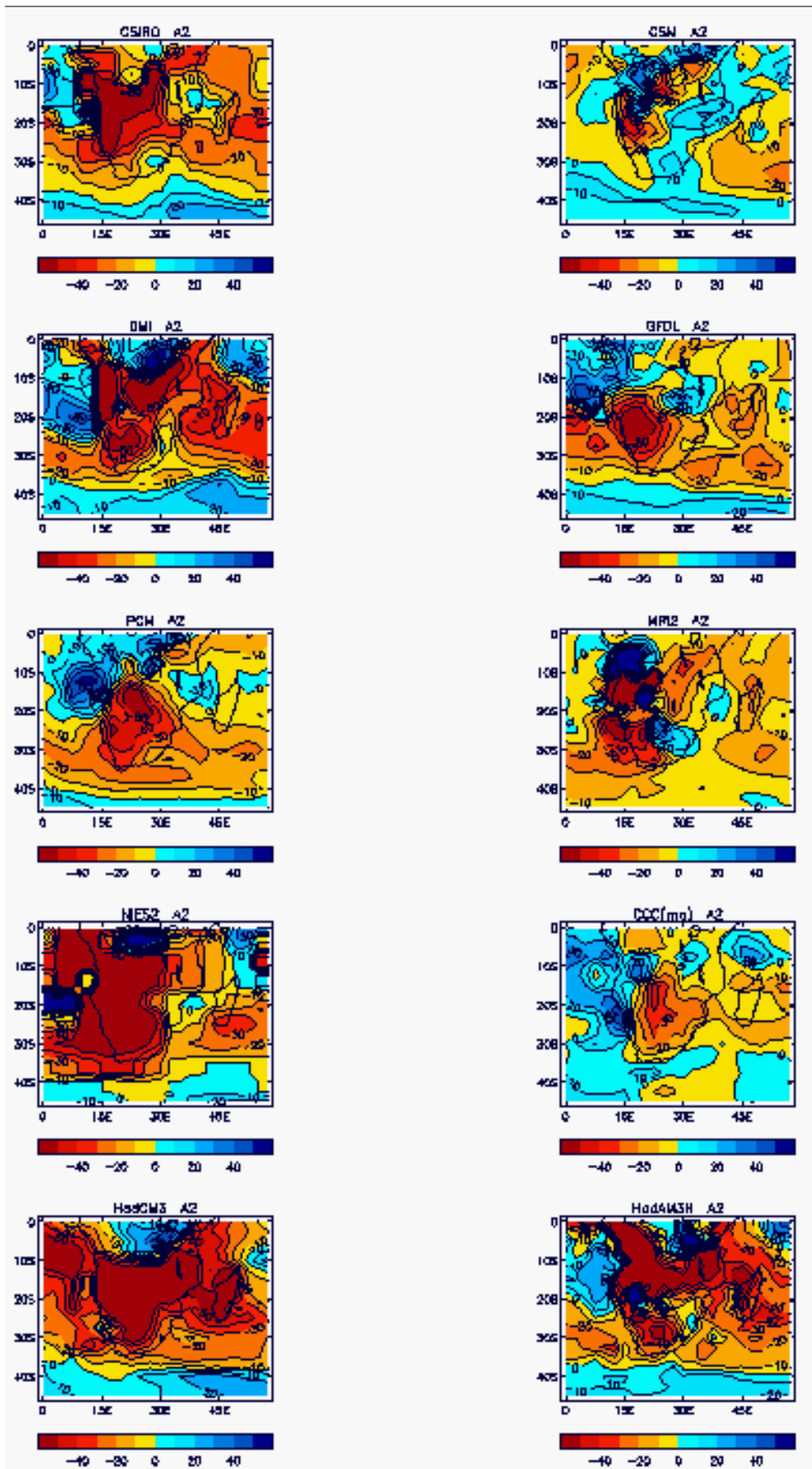


Figure 34: As for Figure 33, but for precipitation (% change) in winter (JJA).

